2013

Navigation & control of an automated SWATH surface vessel for bathymetric mapping

Ketan Rasal
Santa Clara University

SANTA CLARA UNIVERSITY

Department of Mechanical Engineering

Date: January 10, 2013

I HEREBY RECOMMEND THAT THE THESIS PREPARED UNDER MY

SUPERVISION BY

Ketan Rasal

Navigation & Control of an Automated SWATH Surface Vessel for Bathymetric Mapping

BE ACCEPTED IN PARTIAL FULFILLMENT OF THE
REQUIREMENTS FOR THE DEGREE

OF

MASTER OF SCIENCE IN MECHANICAL ENGINEERING

_____

Christopher Kitts, Thesis Advisor

_____

Drazen Fabris, Chairman of Department

Navigation & Control of an Automated SWATH Surface Vessel for Bathymetric Mapping

By

Ketan Rasal

GRADUATE MASTER THESIS

Submitted in Partial Fulfillment of the Requirements
For the Degree of Master of Science
in Mechanical Engineering
in School of Engineering
Santa Clara University, 2013

Santa Clara, California

Navigation and control of an ASV SWATH with dynamic feed-forward control

Ketan Rasal

Department of Mechanical Engineering

Santa Clara University

2013

Abstract

With the abundant amount of water on the earth, the study of underwater terrain plays an important role in the use and sustainability of marine resources. A wide variety of technical systems are used to collect such bathymetric data, and autonomous vehicles are being explored as a manner in which to make this process more cost-effective. Students in Santa Clara University's Robotic Systems Laboratory are contributing to this effort through the development of an autonomous SWATH boat that can create such maps. As part of this thesis work, the navigation and control system of this SWATH boat has been significantly enhanced. This includes refinement of a path-following controller, development of a trajectory controller that sequences desired paths in a Mow-the-Lawn pattern, and the creation of planning tools to generate trajectories based on high-level descriptions of regions to be mapped. This work included exploration of feed-forward disturbance controllers to improve rejection of wind and current disturbances, and it also included a canard control system to trim vehicle pitch in order to increase mapping speeds. These improvements were experimentally demonstrated in multiple field deployments, and the SWATH vehicle is now capable of providing science-quality bathymetric maps.

Keywords: Bathymetry, SWATH, Autonomous Surface Vessel, Navigation Control

Acknowledgements

First and foremost I would like to thank my advisor, Dr. Christopher Kitts for his guidance and dedication towards the students and teaching. I really appreciate his patience in answering my stupid questions.

I would also like to thank everyone in the SCU Robotics System Lab for all the help during my thesis. The deployments were tough and few of them were rough too. Without them I wouldn't have finished all my testing. In this I would like to mention my friend and colleague Thomas Adamek specifically as his help and constant push to get work done played an important role in finishing my thesis. I would also like to thank Alexi for working with us for improving the mapping techniques.

Finally, I would like to thank my family for their support and encouragement throughout my academic career. Without their backing this would not have been possible. Thanks to all my friends for continuously bugging me to finish my thesis, that definitely helped. Last but most importantly, I thank my wife Kavita who has really been a better half of my life throughout this journey. I really admire her constant support and encouragement, thank you.

I thank all the guys on the lakes who come to ask questions about the torpedo looking alien vehicle. Their chat always helped us to relax during busy deployment. I cannot forget the guy who offered us trouts after his bombardment of the doubts about the boat.

Financial support for this work was provided, in part, by NASA through the RETINA program and by the Santa Clara University Robotic Systems Laboratory. I would also like to thank William Kirkwood and his colleagues from Monterey Bay Aquarium Research Institute and Sam Hulme from Moss Landing Marine labs for their support and guidance.

Table of Contents

List of Figures

Chapter 1: Introduction

Seventy percent of Earth's surface is covered by water. The ocean as well as inland lakes and waterways are home for many different species of plants and organisms. These waters are also abundant in natural resources such as minerals. In addition, fresh water sources are the main supplies of water for humans and the crops and animals that they raise. Overall, humans are continuously in search of different ways to make use of the abundant natural resources provided by the Earth's bodies of water.

Knowledge of the physical oceanography of the region is critical in order to efficiently exploit the resources in bodies of water. One of the main parameters of interest is the topography of the bottom of the water body, which is known as bathymetry. Bathymetric information regarding structure and make-up of the floor can be used to understand the local geology, current fields, habitat characteristics, and ecosystems. Because of this, creating bathymetric maps is of great interest for a wide variety of marine applications.

This thesis describes the development of an autonomous boat capable of performing bathymetric mapping. The boat has a novel hull design, making it capable of operating in very shallow water. Furthermore, the automated navigation system allows the boat to operate unattended for hours at a time, making operation very low cost.

1.1 Bathymetric Mapping

Bathymetry is the study of underwater depth of any water body like a lake, slew, river or ocean. Bathymetry is, in its simplest form, the three-dimensional modeling of the floor of a body of water.

Historically, bathymetric mapping was performed by actually measuring the depth of water with poles or weighted lines [1]. Today, airborne LIDAR systems are capable of rapidly generating bathymetric maps over large bodies of water; however, these

operations are expensive, and light absorption in water typically depth-limits such surveys, often in the 10-15 meter range [2].

The primary technology used now-a-days for bathymetric mapping is ultrasound. Within this technical field, developing a basic understanding of acoustics led to echosounders in the 1930s [3]. These systems originated with single acoustic beams of about 5 degrees of beamwidth, but then matured to multi-beam systems [4] which covered far more area compared to the single beam systems. For multibeam systems, beam phase processing techniques are used to estimate the depth of broad swaths of the bottom terrain in a direction perpendicular to the direction of travel of the host vessel. Over the past four decades, this technology has matured, allowing dozens of beams to collectively illuminate swaths that are several times broader than the local water depth [5]. Side-scan sonar systems use a modified architecture that specifically focuses energy in even wider cross-track swaths of area. Parallel to the development of this equipment, the technology also progressed on the software side, allowing the combination of position, platform orientation, and other data to generate regional bathymetric maps with sub-meter resolution.

1.2 Bathymetric Platforms

Mapping systems are deployed on a wide variety of platforms that include manned vessels as well as a variety of robotic platforms. Sonar instruments are accommodated by being mounted in the hulls or on the side of these vessels; on some occasions, they are mounted on a sled that is towed by a piloted ship.

Large scale bathymetric surveys are traditionally conducted using large manned vessels, such as the one shown in Figure 1.1. These ships, however, are neither low-cost nor appropriate for shallow-water surveys. The draft of these vessels poses a danger to themselves and the environment in shallow, semi-navigable waters, limiting the minimum depth of their measurements. As an example of this, a 2008-2009 NOAA bathymetric survey campaign to map Kachemak Bay, Alaska, was limited to depths greater than 20 meters [6].

Figure 1.1: NOAA ship Fairweather in the Gulf of Alaska[6]

Robotic options include Remotely-Operated Vehicles (ROVs), Autonomous Underwater Vessels (AUVs), and Autonomous Surface Vessels (ASVs). ROVs, such as the one shown in Figure 1.2(a), are human piloted, require support ships/crew, and generally operate in localized areas. AUVs, such as the one shown in Figure 1.2(b) are autonomous and can cover much wider areas during missions that can last from days to months; however, it is difficult for them to operate in shallow waters.

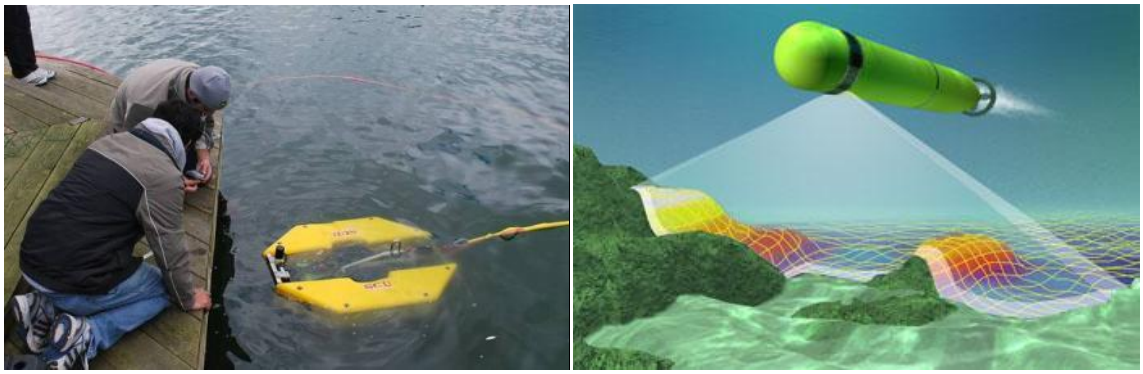

Figure 1.2: (a) RSL ROV Triton in Foster City, CA deployment (*courtesy RSL*). (b) MBARI AUV graphical image. *(courtesy MBARI)*

1.3 Unmanned Surface Vessels

Unmanned Surface Vessels (USVs) are robotic boats that operate on the surface of the water. Because they can perform sophisticated operations on a physically small platform, they are ideal candidates for operating in shallow waters and conducting bathymetric studies.

USVs have been a part of military operations since World War II when they were used as gunnery targets or mine countermeasure drones [7]. The technology has developed a lot since then, and USVs are now used in a vast range of the applications such as sweeping for mines, conducting scientific surveys, towing other marine assets, providing support functions for local underwater vehicles or instruments, and serving as technology research testbeds [8-10]. Most of these USVs are in the form of rigid hull boats, kayaks, inflatable boats, jet skis, etc. Some of the USV chassis are similar to catamarans, and nearly all are less than 15 meters in length. These USVs can be controlled and operated by a remote pilot using a wireless system or via a waypoint or path-following autopilot that uses GPS for position sensing. Most of these systems can stream data wirelessly to an operator if desired.

Since 1993, the MIT Sea Grant College Program has been developing Autonomous Surface Craft (ASCs). The first ASC developed by MIT was ARTEMIS [11]. This vehicle was used to study command and control architectures, navigation systems, and basic data collection techniques, and it successfully proved its autonomous ability and used to collect high-spatial-resolution bathymetry map in some portion of the Charles River in Cambridge, Massachusetts. A follow-on design the ASC ACES (Autonomous Coastal Exploration System), which was developed for better speed, more payload, stability and longer endurance. With advanced features than ARTEMIS, ACES development also was concentrated on high fidelity hydrographic surveys which were carried out in Port of Boston Conley marine Terminal [12-13].

The Springer ASV, an unmanned catamaran, developed by the Marine and Industrial Dynamic Analysis Research Group at University of Plymouth [14], has been used to conduct environmental and geographical surveys in shallow waters. It is a platform for other marine research groups to test their own systems as well. Springer has been used to demonstrate research in pollutant tracking, chemical plume tracing, odor source localization, and many other sensor-drive navigation systems.

From 1998 to 2000, the German Federal Ministry of Education, Research and Technology sponsored the MESSIN project to prototype capabilities in high accuracy positioning, vehicle guidance, and hosting measuring devices in shallow water. The vehicle used a SWATH design, different than the previously described USVs which used catamaran designs. MESSIN used accurate DGPS and compass based navigation, as well as model-based H2 automatic course controller, which allowed the vehicle to perform applications such as depth and current profile measurements [15].

Recently, the Taiwan Ocean Research Institute (TORI) and the Taiwanese National Applied Research Laboratories (NARL) collaborated to develop a USV for inshore marine topography, hydrology, water quality, and meteorological data [16]. This platform integrates Wi-Fi for communication, uses GPS as a positioning system, and communicates data to an onshore control station for immediate acquisition of the data.

Other USVs of note include the following. ROAZ, developed by the Instituto Superior de Engenharia do Porto, is used to conduct shallow water environmental surveys [17]. SESAMO was developed by the Consiglio Nazionale delle Richerche-Istituto di Studi sui sistemi Intelligenti per l'Automazione in Italy for studies of the air-sea interface [18]. DELFIM was developed by the Lisbon Dynamical System and Ocean Robotics Laboratory [19] in order to work cooperatively with an autonomous underwater robot. Recent literature suggests that these systems are now either non-operational or serve primarily as navigation research testbeds [20-24]. All of these have proven their use in multiple research areas, and all have been successfully operated in marine environments.

1.4 SWATH Vessels

The Small Waterplane Twin Hull (SWATH) hull design is often adapted as a means to reduce roll and pitch disturbances. This is of particular interest for vehicles performing bathymetric operations given that such disturbances complicate sonar data processing and induce errors in the reconstruction of maps. SWATH boats employ a dual hull design with a minimal hull volume at the waterline. The effect of a small hull waterline is a minimal change in buoyancy due to wave interaction with the hull, resulting in a platform with excellent wave disturbance rejection and natural stability in pitch and roll. Schematic explanation for this is shown in Figure 1.3. SWATH design provides more space for equipments and load carrying capacity as well [25-29].

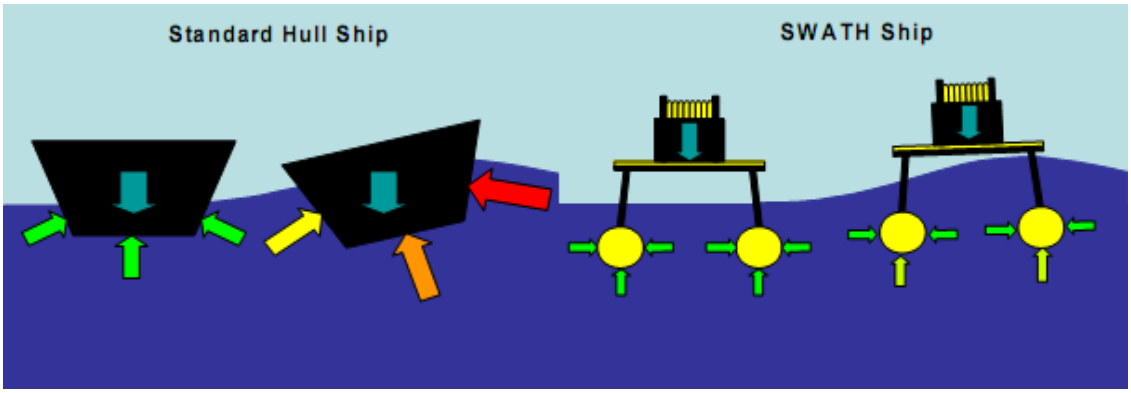

Figure 1.3: Wave effect on standard hull against SWATH hull [25].

The original SWATH boat concept was patented in 1905 [30]. There have been about 50 SWATH boats developed until now, and they are in service for conducting oceanographic surveys [31,32], mine hunting and ordinance disposal [33,34], and ferrying passengers [28,35]. About 80% of these ships are over 100 feet in length, and nearly all are longer than 40 feet [27]. In particular Lockheed Martin's Kilo Moana, shown in Figure 1.4, is used for bathymetric mapping, and with a set of two multibeam sonars its mapping range varies from 10mtr to 11000mtr [36]. It provides the opportunity to explore the topography of reasonably shallow waters, such as off the coast of Hawaii; however, its 185 foot long length makes navigation in small water bodies difficult.

Figure 1.4: Lockheed Martin's Kilo Moana research vehicle[36]

Through a partnership between the Santa Clara University's (SCU) Robotic Systems Laboratory (RSL) and the Monterey Bay Aquarium Research Institute (MBARI), a SWATH boat, shown in Figure 1.5, has been developed as a platform for conducting automated bathymetric operations. The project started in 2005 and entered science-quality operations in Summer 2011 [37]. With 3.4 meter in length and about 1.6 meter in width and height, this boat can easily maneuver in small, tight, and shallow areas.

Figure 1.5: Santa Clara University RSL lab's SWATH boat, at one of the deployment in Emerald Bay, Tahoe, CA[37]

Like many other USVs SWATH uses GPS for position sensing, and it can be controlled either by a remote pilot or with automated path following algorithms. The commands are computed using a shore-based computer and are sent to the boat using a wireless communication system. As the boat navigates through an area of interest, its Delta-T multibeam sonar head, mounted in the hull, a precision Trimble GPS sensor, and an Attitude Heading Reference System (AHRS) sensor log data that is post-processed to create mapping products. During mapping sessions, the passive hull design of the boat helps to minimize wave-induced pitch and roll disturbances. However, mapping performance is generally improved if active controllers can keep the boat on its prescribed path and can eliminate steady-state pitch errors resulting from the torque created by the vehicle's operating speed.

1.5 Project Statement

The objective of this research project was to develop improved navigation and control capabilities for the SCU SWATH vehicle in order to improve its ability to cost-effectively perform bathymetric operations. This included the refinement of the vehicle's path-following controller and the creation of high-level path generation interfaces. It also included experimentation with a dynamic feed-forward controller to counteract wind disturbances and also with a canard controller to trim velocity-induced steady-state vehicle pitch errors. Elements of these controllers were integrated into the vehicle's operational control software and were used in multiple science field operations.

Specific results included improved path-following performance that reduced cross-track error to less than one meter during ideal conditions. For windy conditions, the feed-forward controller reduced errors more than half. Furthermore, the use of active trim control showed the ability to nearly double the vehicle's operational speed. Considerable work was also performed in order to refine techniques for the creation of bathymetric maps based on the sensor data collected during these operations; this allowed maps to be created with a depth measurement repeatability of 0.286 meters at one standard deviation, which exceeds the typical industry requirement to qualify as a science-quality result. The result is an improved control and data processing system that has proven its value while conducting real operations with world-class science partners.

Chapter 2: SWATH – Design and Development

Santa Clara University's (SCU) Robotics System Lab (RSL) is a multidisciplinary lab which conducts collaborative research in the field of robotics operating on land, in the water, in the air and in space [38]. Through collaborations and sponsorships from partners such as NOAA, the Monterey Bay Aquarium Research Institute (MBARI), NASA, Lockheed Martin, and BMW, RSL students develop new robotic devices and control techniques for particular applications. Further, these applications are tested on real robots to verify their validity in the real world. Many such applications are been developed and tested in RSL to date. Some of the robotic systems used within the lab are shown in Figure 2.1

Figure 2.1: Robotic systems used by RSL (a) Wheeled Robots – Amigo bots, Pioneers, (b) ROV – Triton, (c) Airplanes, (d) Satellite

2.1 The SWATH Autonomous Boat

One of the RSL's robotic systems is the SWATH boat for bathymetric mapping. The original vision for the SWATH boat was to provide enhanced pitch/roll stability in very shallow water and to host science capable equipment for automated missions lasting up to 8 hours.

In the years 2004-2005, with the help of MBARI, the development of SWATH was started, with the first objective being the development and stability testing of the SWATH chassis [39]. Follow-on projects were carried out to add batteries, thrusters, a navigation system, and a suite of bathymetric mapping equipment. The current as-built version of the boat consists of about $5,000 of equipment invested in the main vehicle

with another $50,000 of mapping sensors constituting the bathymetric payload. Figure 2.2 shows SWATH operating in one of the mission in Lake Del Valle, CA. The SWATH system includes an off-board control station and on-board subsystems for the hull, vehicle electronics, and payload components.

Figure 2.2: RSL SWATH boat in one of the deployment at Lake Del Valle, CA.

2.2 SWATH Hull Design

A SWATH design was specifically selected to improve the stability of the boat. As mentioned in previous chapter, this design is much stable in roll and pitch given wave disturbances. In a small and unmanned form, the SWATH design also supports operation in very shallow water, which was a specific desire for this project.

The boat's chassis is made up of two pvc hulls with fiberglass ends joined to an aluminum honeycomb platform with two vertical struts on each side. Through stability testing, the strut angle was empirically set to 20^0. To improve the water displacement ratio, the struts were covered with medium density polyurethane foam, which was encased in a fiberglass shell to increase impact resistance and prevent water absorption. The hull's rigidity was improved by adding cross steel bracing from each strut to the

other side of the platform [25]. The final design of SWATH is 3.4 meters long, 1.3 meters tall, 1.3 meters wide platform weighing 360kg in total.

2.3 SWATH Components and Electronics

In the second stage of construction, functional components like batteries, thrusters, and other electronics for navigation were installed on the boat. Batteries, science equipments and thrusters are also mounted within the pontoons. Navigation and communication equipment are mounted on the deck. The boat also has a ballast system, two canards for pitch adjustment, and a winch for lowering alternative payload sensor packages. Figure 2.4 shows the location of various components as installed on the boat. Figure 2.3 shows the architecture of these functional systems on-board the boat.

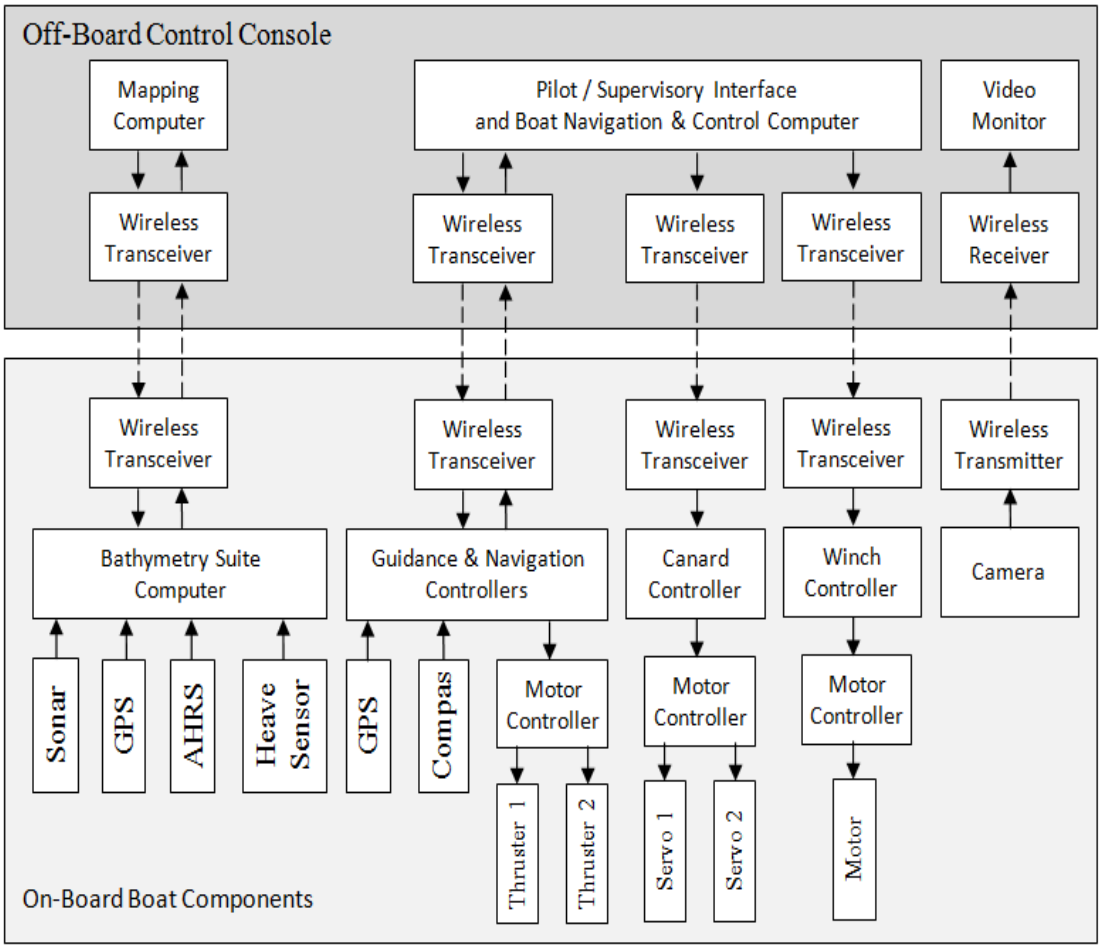

Figure 2.3: Component block diagram for SWATH components [37].

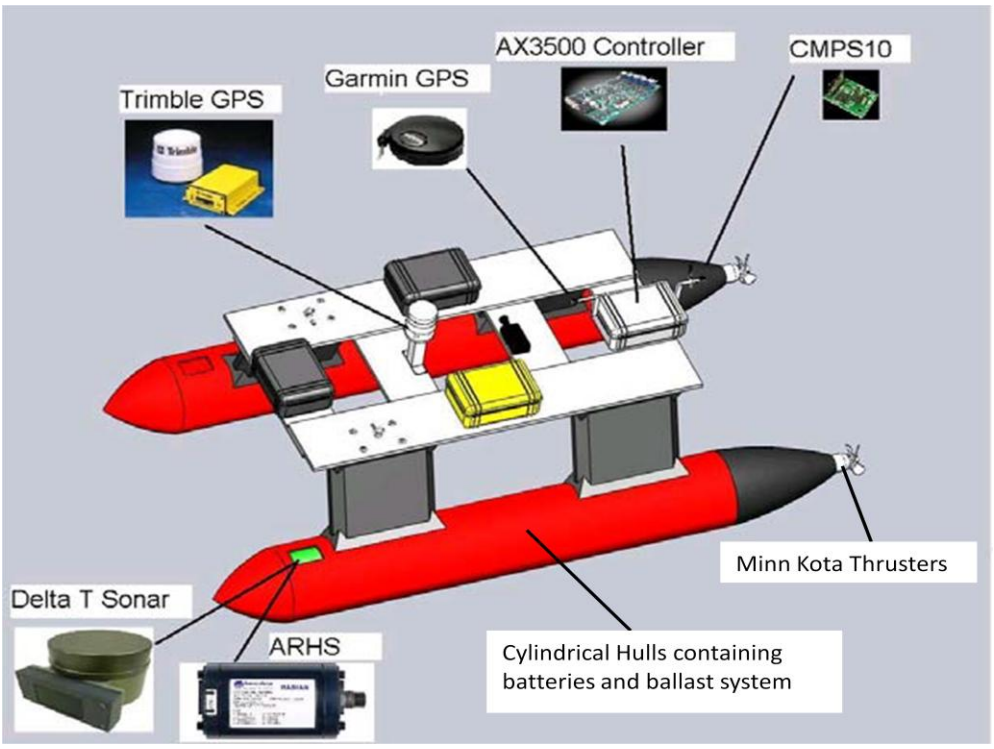

Figure 2.4: SWATH boat mechanical configuration and component location [37].

The batteries were installed in the pontoons in order to lower the boat's center of mass, as shown in Figure 2.5. The batteries are enclosed in a 3/8" plastic water tight box with a 3/8" polycarbonate lid and sealed with 1/8" latex rubber and 1/4" bolt closures [39]. These were tested for non-leaking at 1 meter up to 72 hours in accordance with IP-68.

Figure 2.5: Batteries mounted in water tight containers placed in the hull of SWATH[39]

For propulsion, the boat uses two Minn Kota RT55 electric trolling motors. These thrusters are installed at the aft end of each pontoon, and they provide 55 pounds of thrust each. This mechanical configuration allows the boat to be controlled via a differential drive strategy. The differential commands are given to the thrusters by a RoboteQ AX3500 motor controller. This brushed DC motor amplifier converts the commands received from an on-board computer into individual drive commands for the thrusters.

Position data for navigation is provided by a Garmin 18 GPS receiver which is a low cost, off the shelf unit. It has refresh rate of 5Hz and rms accuracy of +/-3 meters. Heading data is provided by Deventech CMPS10 compass with rated error of +/-3 degrees and refresh rate of 10Hz. The boat's on-board navigation computer is made up of two BasicX-24 embedded controllers, each of which uses an 8-bit RISC ATMEGA8535 processor and has 32 KB of EEPROM and 400 bytes of RAM. This processor executes a multi-tasking version of the BASIC programming language and is capable of executing 83,000 lines of code per second. The controller collects the telemetry data from GPS and compass and communicates it to off-board computer using a long range 19,200 kbps serial radio modem. Drive commands are generated by the off-board computer by polling a pilot joystick or by using an error-driven PID controller for waypoint, trajectory, or path-following control. These commands are wirelessly relayed back to the boat's on-board controller and routed to individual motors through the RoboteQ motor driver.

SWATH stability is improved by a pair of differentially articulating canards mounted at the front of the boat. SWATH tends to pitch forward with an increase in speed, and that is a limiting factor for mapping speed. The main function of the canards is to provide pitch-trimming torques that can be changed for different speeds of the boat. The canards, shown in Figure 2.6, are controlled by two linear actuators with a position feedback. This position data, as well as platform pitch and roll data provided by the CMPS10 compass module, is collected by an Arduino Uno and communicated to an off-board computer through an XBee radio modems which use 2.4 GHz frequency and transfer data at the rate of 250 kbps. Actuator commands are then calculated by the off-board computer and are communicated back through the XBee radiomodem to the

Arduino. The Arduino controls the canard actuators via a RoboteQ AX1500 motor control board.

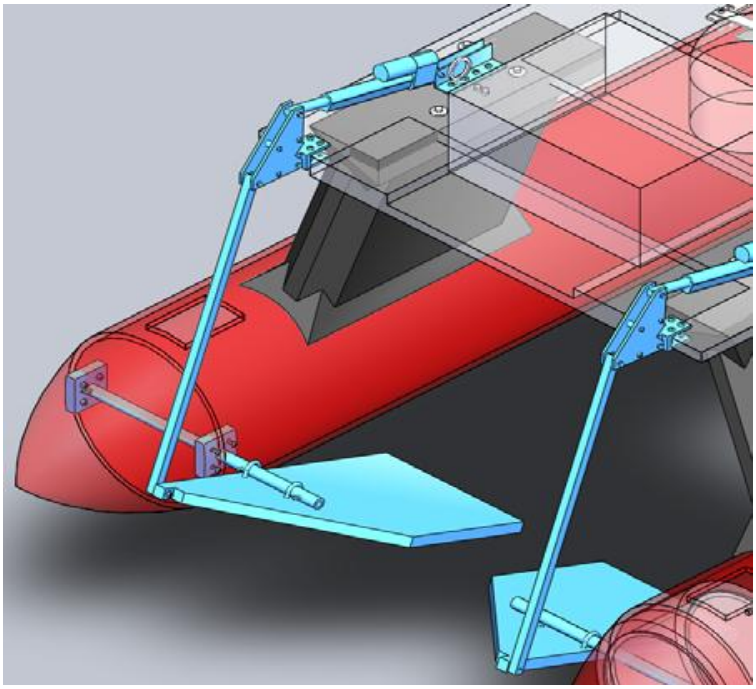

Figure 2.6: Graphical view of Canards mounted at the front of SWATH.

2.4 SWATH mapping equipment

SWATH uses an Imagenix 837 "DeltaT" multibeam imaging sonar for bathymetric mapping. This unit is capable of 20 pings per second and a range of 100 meters. The generated images of the bottom are then linked with location coordinates received from a high precision marine-grade Trimble GPS unit. A Crossbow Attitude Heading Reference Sensor is used for roll and pitch correction of the mapping data. In addition, a Teledyne Heave sensor is also used to measure heave experienced by the boat, but this is not yet in use for generating maps. The time stamped data from all the sensors is collected on a separate payload computer during real-time operations. This data is processed after completion of each mission using the MB System mapping software suite, and bathymetric maps are generated.

Chapter 3: Navigation and Control

The main objective of this thesis was to design and develop navigation and control techniques to enhance the ability for the SWATH boat to generate bathymetric maps. The boat has several control modes, to include a human-piloted mode, a heading control mode, a waypoint control mode, and a path following mode. To enhance operation, modifications and improvements to the path following mode were made, and higher level control and specification techniques were developed to allow simple "mow-the-lawn" operation.

3.1 Dynamics of SWATH

To aid in the design a SWATH navigation controller, a model of the vessel was generated. While a 6 degree of freedom dynamic model [40] can be generated in order to capture the comprehensive effects of the forces and toques acting upon the vehicle, this level of detail was unnecessary for the objectives of this project. We considered a simplified version of the translational dynamics, using numerous assumptions such as linear behavior about operating points, decoupling between translation and orientation, vehicle symmetry, and so on.

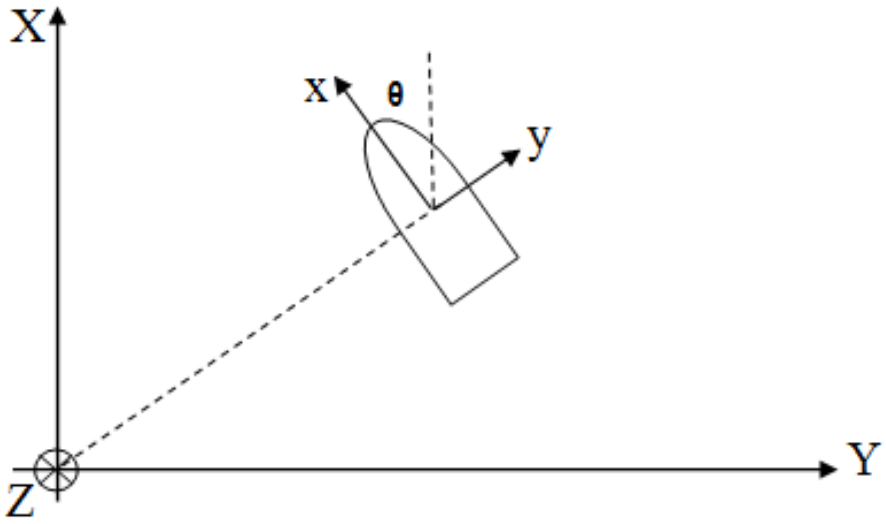

Figure 3.1: ASV reference frame.

Assuming the center of mass at the center of the ASV, the local frame and global frame for the ASV are defined as shown in Figure 3.1. A first order model for the relationship between actuator commands and translational/rotational velocity was assumed and experimentally determined. This was justified by assuming zero dynamics for the actuators (which are more than an order of magnitude faster than the boat itself), and assuming a first order relationship between propeller forces/torques and vehicle motion.

As described before, SWATH is controlled by differential drive strategy. Each thruster creates an independent force on the boat which causes the boat to move forward and/or turn. Actuation starts with PWM commands to the motor controller; these define the equivalent voltage applied to the thrusters, which, in turn cause rotation that leads to the generation of forces. This is depicted is Figure 3.2.

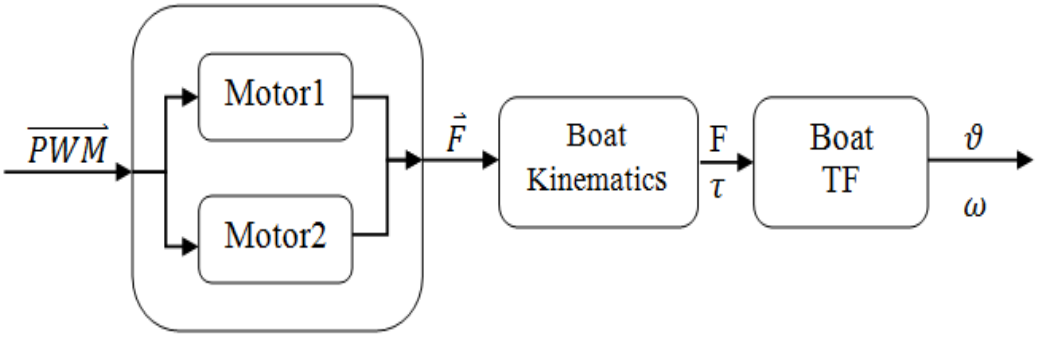

Figure 3.2: Boat model block diagram

Experimentally, relationships between the input %PWM commands, the generated forces, and the resulting boat velocities were determined. Data collected for three tests and averaged to get final relationship. To measure the force vs %PWM relationship, the boat was held stationary with a force sensor, and force was measured for different %PWM levels with both thrusters running. Figure 3.3a shows the measured force vs. %PWM relationship. To measure Velocity vs. %PWM, the boat's steady state translational velocity was measured at different %PWM levels. Figure 3.3b shows the data for steady state velocity (m/s) vs. the %PWM level.

Using this data, the following relationships are formulated:

$$Force\ (N) = 144.2 * \%PWM - 1.826 \sim 144 * \%PWM \tag{3.1}$$

$$Velocity\left(\frac{m}{s}\right) = 1.221 * \%PWM + 0.0303 \sim 1.22 * \%PWM \tag{3.2}$$

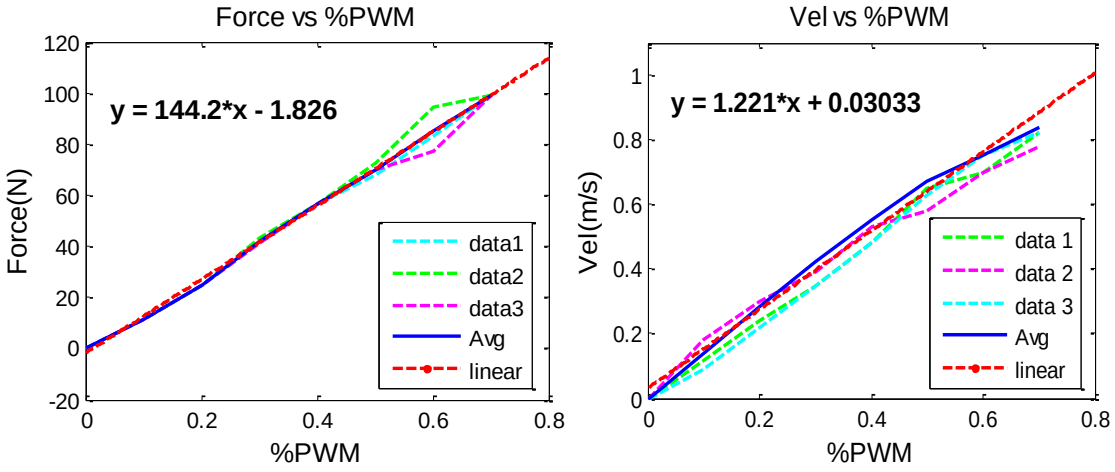

Figure 3.3: (a) Relationship between Force and %PWM, (b) Relationship between Velocity and %PWM

Thus the force created by PWM on the boat moves the boat. Due to differential drive strategy the boat will either move forward, if both the forces are equal, or turn depending on the force difference in the propellers. To get the total force and torque acting on boat kinematic function is derived as follows

$$Fb = F1 + F2 \tag{3.3}$$

$$\tau = -F1 * \frac{Wb}{2} + F2 * \frac{Wb}{2} \tag{3.4}$$

Where "F1" and "F2" are propeller forces and "Fb" is total force on boat. "τ" is torque on boat and "Wb" is width of the boat.

Experimental data was also used to derive the time constant for the system. The boat was commanded with a constant forward velocity step input from a standstill

position. The resulting velocity profiles for various velocity commands are shown in Figure 3.4. It can be seen that, for all cases, a steady state speed is achieved after approximately 25 seconds. Assuming that the settling time is approximately 5 time constants, the time constant is approximately 5 seconds. From the curves in the figure, the steady state gain was roughly approximated to be about 1. This led to the transfer function for the boat as follows.

$$boat\ T.F. = \frac{1}{5s+1} \tag{3.5}$$

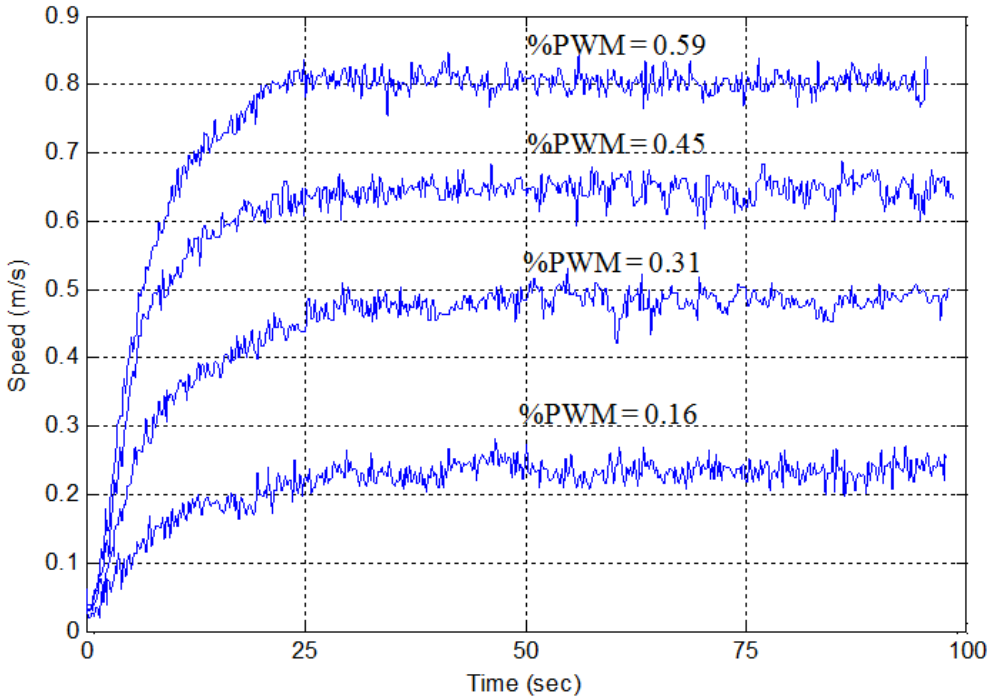

Figure 3.4: Constant forward velocity test results

3.2 Cross-Track Control Strategy

For bathymetric mapping, a path-following approach with a constant forward thrust is preferred as a navigation strategy [37]. The overall path used for a mapping operation consists of numerous path segments that are either linear or semi-circular. To eliminate cross-track error, differential torque compensation is used.

The cross-track controller relies on an inner heading control loop, such that the error in the heading defines the torque required for the boat. The control law for heading controller can be stated as follows

$$e_h = \theta_{des} - \theta_{act} \tag{3.6}$$

$$\tau = K_{hp} * e_h + K_{hd} * \frac{d\,(e_h)}{dt} \tag{3.7}$$

Where, K_{hp} and K_{hd} are heading control PID gains.

Compass heading is converted from 0 to 360 degrees to -180 to +180 degrees. Thus the error between two angles is also converted to -180 to +180. Using this desired torque and the nominal translational boat force, inverse kinematics are used to compute the desired forces for each of the boat's thrusters. These are then converted to the necessary %PWM commands. The heading control loop is explained by Figure 3.5. A graphical snapshot of the Simulink controller used for field test is shown in Appendix B.

$$F_1 = \frac{F_b}{2} - \tau \tag{3.8}$$

$$F_2 = \frac{F_b}{2} + \tau \tag{3.9}$$

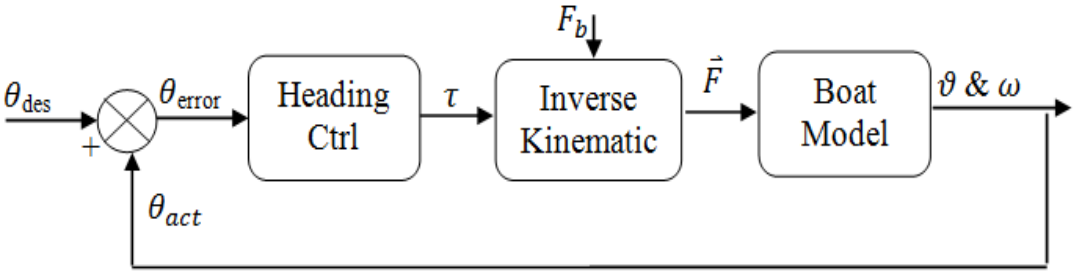

Figure 3.5: Heading Controller block diagram

The cross-track controller uses the heading controller as an inner loop by specifying an instantaneous heading command. The nature of the cross-track controller varies depending on whether the current path segment being followed is a straight line or a semi-circle (used to turn from one straight line to the next when "mowing-the-lawn").

3.2.1 Line Controller

In general, the cross-track strategy can be explained by Figure 3.6, which shows the case of a line segment path. Cross-track error is the perpendicular distance of position of the boat reported by GPS from the current path segment. The path is defined by the endpoints of the current path segment being executed and the direction of travel. The cross-track control strategy specifies that the desired heading that matches the path bearing plus or minus a corrective heading term based on cross-track error. Based on this, the cross-track controller feeds a desired heading command to an inner loop boat heading controller.

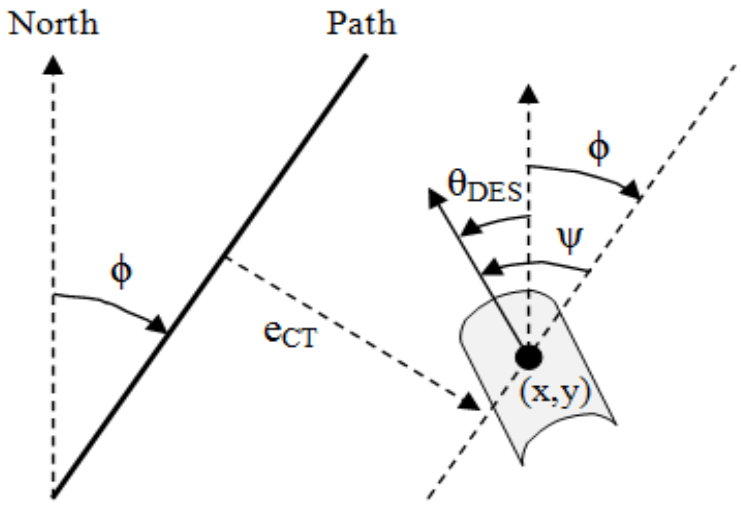

Figure 3.6: Cross-track control strategy, where ∅ is bearing of path, e_{ct} is cross-track error, ψ is corrective turn angle, θ_{DES} is desired heading, (x,y) is boat location, K_{CT} is gain. [37]

The control strategy is explained by following equations

$$\psi = K_{CT} * e_{CT} \tag{3.10}$$

$$\theta_{DES} = \phi - \psi \tag{3.11}$$

This strategy is depicted as a control block diagram in Figure 3.7.

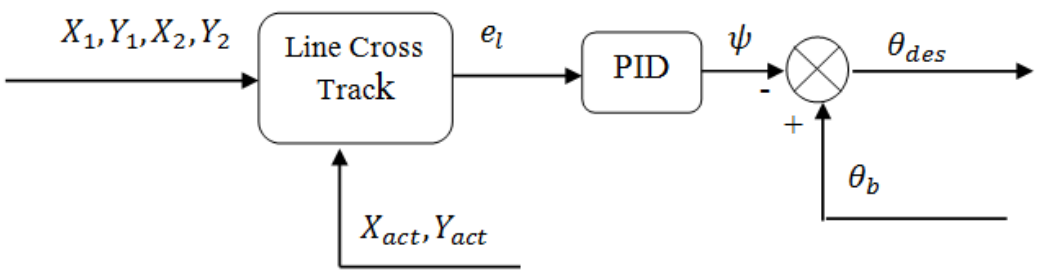

Figure 3.7: Line Controller block diagram

A graphical snapshot of the Simulink controller used for field test is shown in Appendix B. The formulae used are explained as follows.

$$L_l = \begin{bmatrix} X_2 \\ Y_2 \end{bmatrix} - \begin{bmatrix} X_1 \\ Y_1 \end{bmatrix} \tag{3.12}$$

$$L_a = \begin{bmatrix} X_2 \\ Y_2 \end{bmatrix} - \begin{bmatrix} X_{act} \\ Y_{act} \end{bmatrix} \tag{3.13}$$

$$e_l = \frac{det[L_l \quad L_a]}{norm(L_l)} \tag{3.14}$$

$$\theta_{des} = \theta_b - K_l * e_l \tag{3.15}$$

Where, K_l is line controller gain. This error is converted to desired angle for the boat using equations 3.15. This is then used as input for heading controller.

3.2.2 Circle Controller

The Circle Controller uses the same basic cross-track strategy, but the error is calculated along the desired circular path. Since the boat moves in circular path, it's bearing constantly changes and is defined as a function of the position of the boat. The error is the difference between radius (R) and the distance of the boat (Pos_b) from center of the circle (C_p). The desired bearing (θ_b) of the boat is always tangential to its desired radial position on the circle at any given time. This is explained in Figure 3.8.

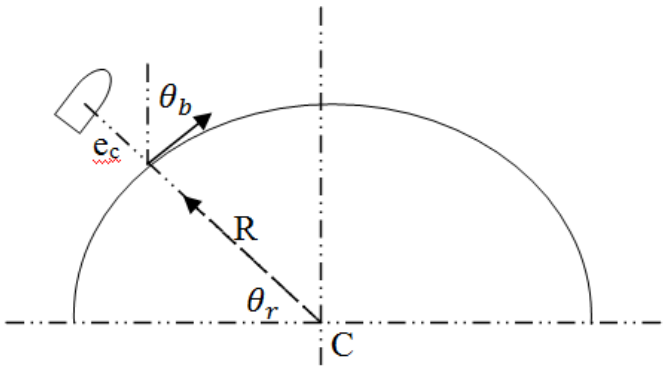

Figure 3.8: Cross-track control strategy for Circle Controller

The basic block diagram for the controller is shown in Figure 3.9.

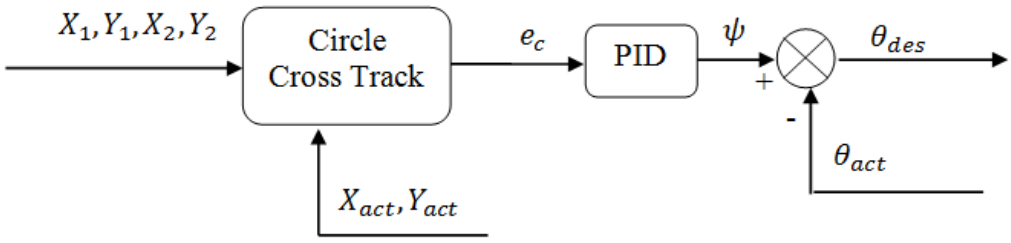

Figure 3.9: Circle Controller block diagram

A graphical snapshot of the Simulink controller used for field test is shown in Appendix B. The control law can be explained by following equations. First the distance of boat is calculated from the center of the circle with coordinates (X_c,Y_c). Then the error is calculated by subtracting it from the radius of the circle.

$$Pos_b = \sqrt{(X_{act} - X_c)^2 + (Y_{act} - Y_c)^2} \tag{3.16}$$

$$e_c = R - Pos_b \tag{3.17}$$

Desired bearing for the boat is perpendicular to $\overrightarrow{R}$ at any given point of time.

$$\theta_b = \theta_r + \pi/2 \tag{3.18}$$

This error is converted to desired angle for the boat using equations 3.17. This is then used as input for heading controller.

$$\theta_{des} = \theta_b - K_c * e_c \tag{3.19}$$

Where, K_c is Circle controller gain.

3.3 Mow-the-lawn Strategy: Meta Controller

Bathymetric mapping is performed using a Mow-the-Lawn path-following strategy, as shown in Figure 3.10. This strategy is implemented via an automated controller which directs the boat to follow a series of parallel lines that are evenly spaced across the region to be mapped. At the end of each line segment, the boat follows a semicircular path in order to follow the next line segment in the opposite direction. As a matter of practice, each line segment is extended beyond the region of interest prior to the semicircular turn by an amount to ensure that the boat properly tracks the straight path after each turn, prior to re-entering the region of interest. The mapping region is defined through a higher level Mission Planning process, described in Section 3.4.

The meta-controller first converts the definition of the region of interest into a matrix of points representing a sequence of path segment endpoints. During real-time operation, the meta-controller controls the boat's movement in the mapping region by sequencing through the individual path segments and invoking the appropriate cross-track controller using the appropriate parameters for each segment.

3.3.1 Representing Path Segments

From the planning process, the region of interest is represented by a starting location, a length and width of the mapping region, and an orientation of the mapping region. An indication of the route option (lengthwise or lateral) and a linear safety distance are also prescribed. In addition, the spacing between the line segments, which is a function of the depth of the mapping region and angle of beams, is determined so as to get 50-75% of overlap of the sonar beam and fed to this function.

Given the high level description of the region of interest, the path segment sequence is generated in the manner depicted by the flowchart in Figure 3.12. Path segments are encoded by representing their endpoints sequentially in a matrix of the form:

$$M = \begin{bmatrix} Y_1 & Y_2 \\ X_1 & X_2 \ldots \\ 1 & 1 \end{bmatrix} \tag{3.20}$$

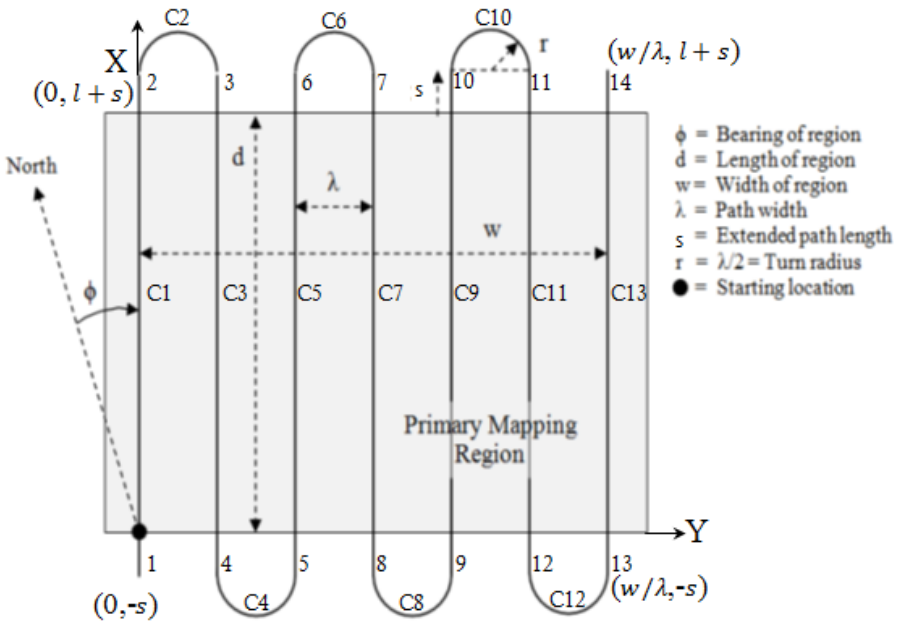

Figure 3.10: Example of mow-the-lawn path for mapping operation. Numbers 1-14 are the end points of the path segments defined as C1 to C13 [37].

Note from Figure 3.10 that the global (X,Y) frame has the X-direction aligned vertically and the Y-direction aligned to the right. The first two points are represented in local coordinates as $\begin{bmatrix} 0 \\ 0 \end{bmatrix}$ and $\begin{bmatrix} 0 \\ l \end{bmatrix}$, where "$l$" is the length of the region of interest. The linear safety distance is added by offsetting these two points by "s", the safety distance, such that the first two points become $\begin{bmatrix} 0 \\ -s \end{bmatrix}$ and $\begin{bmatrix} 0 \\ l+s \end{bmatrix}$. For the second line segment, note from figure 3.10 that point 3, the next point in the path sequence, is the "top" point on the map, with point 4 on the bottom; these are offset in the Y direction by a distance "λ",

which is the spacing between paths. Accordingly, line segment 2 (C3) is defined by points 3 and 4, which are represented as $\begin{bmatrix} \lambda \\ l+s \end{bmatrix}$ and $\begin{bmatrix} \lambda \\ -s \end{bmatrix}$, respectively. The matrix continues for w/ λ path segments, since this is the number of segments that are required given the width region of interest and the desired path spacing:

$$M = \begin{bmatrix} 0 & 0 & \lambda & \lambda & 2\lambda & 2\lambda & w/\lambda & w/\lambda \\ -s & l+s & l+s & -s & -s & l+s \ldots & -s & l+s \\ 1 & 1 & 1 & 1 & 1 & 1 & 1 & 1 \end{bmatrix} \tag{3.21}$$

The M matrix now represents the nominal path structure for the region of interest. However, the bearing of the mapping area has yet to be accounted for, and the options of starting corner and path mirroring have yet to be applied.

Path mirroring, described in more detail in Section 3.4, is an option in which the path shown in Figure 3.10 is mirrored about the X-axis. All possible permutations of path overlays for a region of interest can be compactly represented by a region bearing and a mirroring option. The path sequence in Figure 3.10 is nominal (e.g., not mirrored); a mirrored version would have the boat turning to the left at the end of its first straight-line segment, with the region of interest falling in the +X/-Y quadrant. Given M as previously defined, whether the map is mirrored or not is accounted for by the following transform:

$$M' = \begin{bmatrix} m & 0 & 0 \\ 0 & 1 & 0 \\ 0 & 0 & 1 \end{bmatrix} * M \tag{3.22}$$

Where, m=1 if the path is to remain as shown in Figure 3.10, and m=-1 if it is to be mirrored. The bearing of the mapping region and the selection of starting point (e.g., the corner of the map at which the boat starts) is accounted for using the following transform:

$$M_F = \begin{bmatrix} cos\emptyset & sin\emptyset & Y_{st} \\ -sin\emptyset & cos\emptyset & X_{st} \\ 0 & 0 & 1 \end{bmatrix} * M' \tag{3.23}$$

Where, $\emptyset$ is the bearing of the region of interest and $\begin{bmatrix} Y_{st} \\ X_{st} \\ 1 \end{bmatrix}$ are the coordinates of the starting location.

3.3.2 Real-time Path Sequencing

From the path representation process detailed in Section 3.3.1, the M_F matrix is produced, encoding the local coordinates of the sequence of path points. For real-time control, the meta-controller keeps track of the current path segment, and from the matrix provides the appropriate set of path points to the appropriate cross-track controller, switching between the line controller and the circle controller.

Upon initiation, the boat is driven towards the start point and then controlled to follow the first path segment, denoted as C1 in Figure 3.10. To switch from the first linear segment to the second semi-circular segment, two conditions must be met. First, the boat must be within a meter of the line segment from points 2 and 3 (given that 1 meter is the approximate precision of the GPS signal). Second, the boat's heading must be within some range (+/-50 degrees is typical) of the bearing of the first line segment. With these conditions met, the meta-controller latches the sequence to segment two, switches to the circular cross-track controller, and provides the controller with the appropriate endpoint locations. The boat then follows segment C2, guided by semicircle controller. When the boat is once again within 1 meter of the points 2-3 line segment but now with a 180 degree change in heading (+/- a nominal 50 degrees), the meta-controller switches back to the line cross-track controller, providing it with the locations of the endpoints of third path segment C3. This process continues until the boat is on last segment of the path. The integration of the meta-controller with the path controller is shown in Figure 3.11. A graphical snapshot of the Simulink controller used for field test is shown in Appendix A.

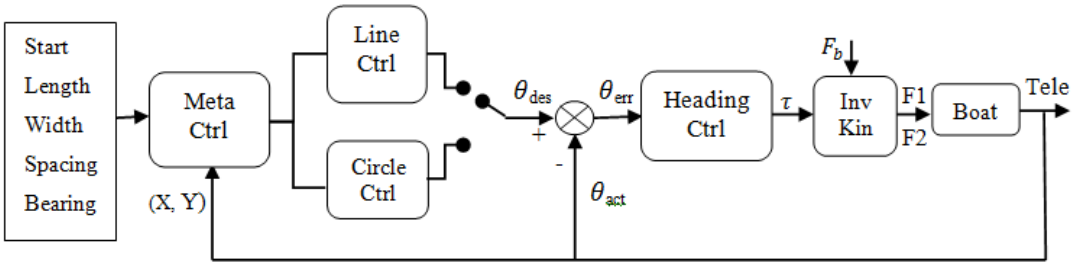

Figure 3.11: Meta Controller block diagram

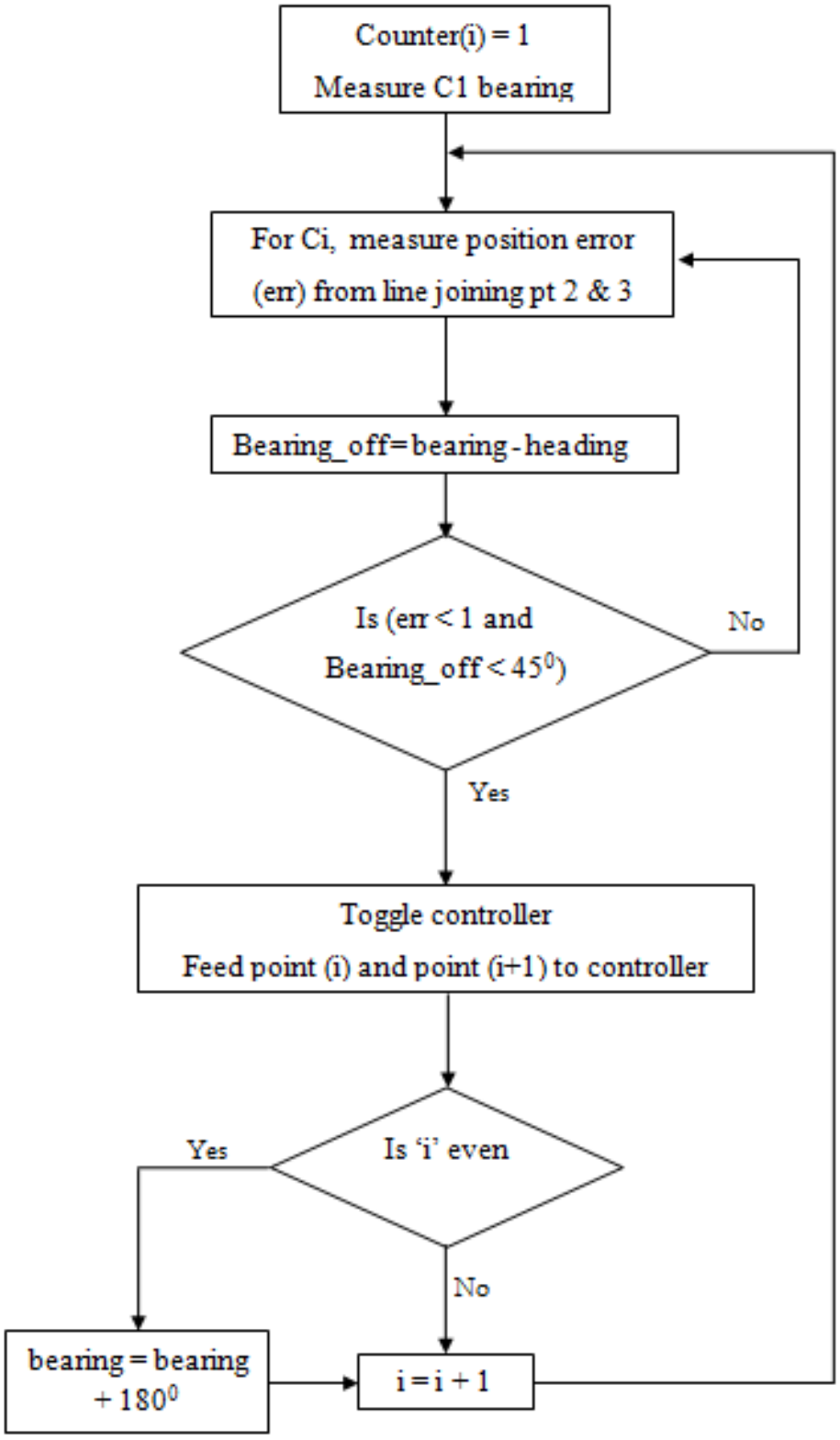

Figure 3.12: Flow Chart of Meta Controller

3.4 Mission Planning

The purpose of the mission planning tool is to provide the required input parameters to the meta-controller based on the customer's description of the region to be mapped. Through our experience with real customers while planning and executing real mapping missions in the field, it became clear that there are a variety of "convenient" ways in which the customers provide a description of the region to be mapped. As a result, the mission planning process and tools were developed to support multiple customer descriptions while ultimately converting this information into the necessary meta-controller inputs.

In the current mission planning framework, four specification approaches for the region to be mapped are supported. We note that all can be defined either in local boat coordinates or via a global frame using latitude and longitude coordinates. The four ways to currently define a region of interest, as shown in Figure 3.13, are:

1. Specify the length, width and orientation of the mapping region, along with a start point at a corner of the region of interest.
2. Specify three corners of the region of interest.
3. Specify the length, width and orientation of the mapping region, along with a center point.
4. Specify the length, width and orientation of the mapping region, along with a start point at the midpoint of the long side of the region of interest.

Meta-controller works in local coordinate system. So for each mission a local coordinate system is defined at the beginning of the mission by calibrating a robot. After first run, customer has an option to keep the local frame same as the first run during the mission or to change the local frame for the new run. Thus an option to calibrate the robot for the mission is provided.

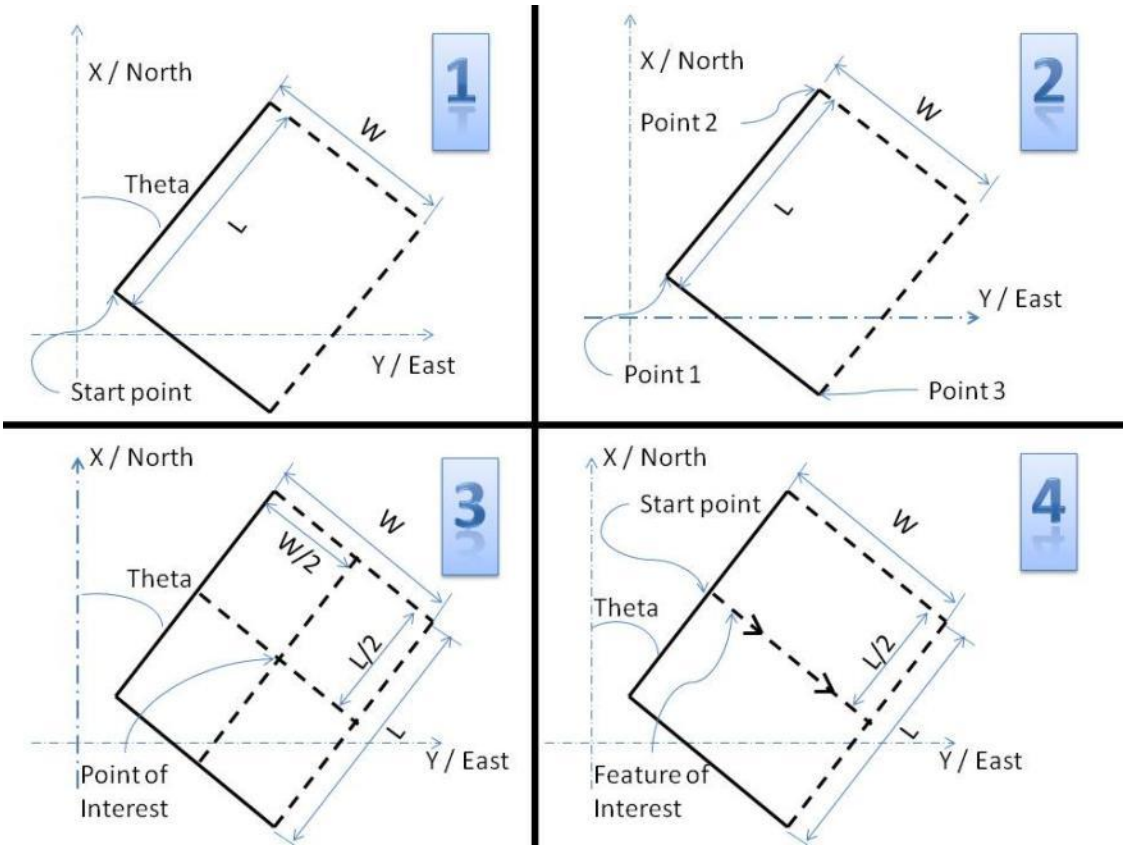

Figure 3.13: Choices to define region of interest

With the region of interest defined, a mow-the-lawn pattern is selected. The options here, shown in Figure 3.14, define the corner in which mapping starts as well as the relative orientation of the straight line paths within the mapping region. From a processing perspective, the underlying math exploits the symmetry of the relative orientation options, with a flag specifying if the baseline path description should be mirrored, or not, as described in Section 3.3.1. It is worth noting that while the customer sometimes does not explicitly define the route orientation, this choice is often made in order to have the straight line paths run perpendicular to depth contours.

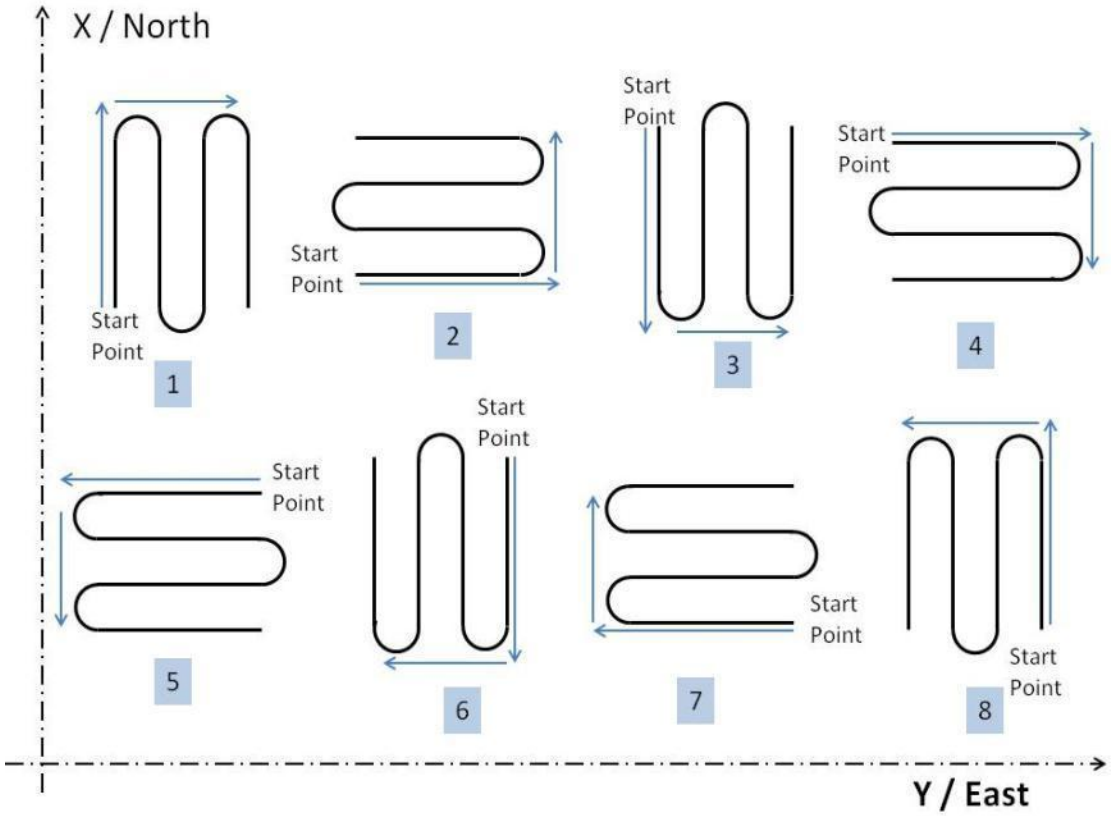

Figure 3.14: Options for the movement of boat along the desire path

Using the above two options final function, from four options, is selected which converts all the data provided to the parameters used by meta-controller. The general flow chart is explained in Figure 3.15.

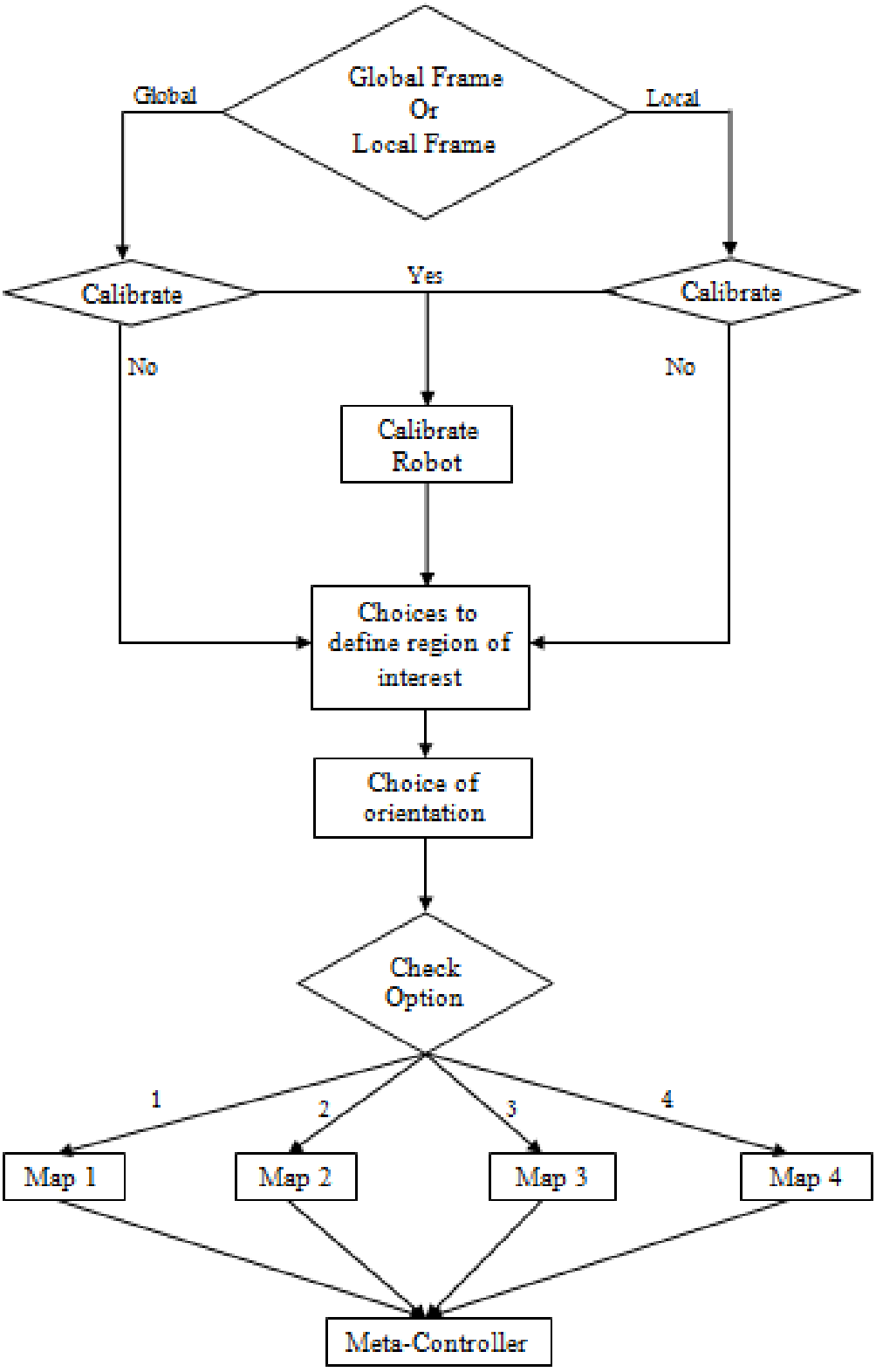

Figure 3.15: Flow-chart for mission planning algorithm

3.5 Navigation Performance of SWATH

Thus, the obtained controller is tested for different conditions, orientations and is verified using simulation. The main condition was to test the working of the controller in different quadrants of the frame. Various starting points for path are used with different starting point and different starting orientation of the boat. In every quadrant multiple orientations of path are also tested. Conditions for flipping the path and mirroring are also checked. Few of the Simulation results are shown in Figure 3.16.

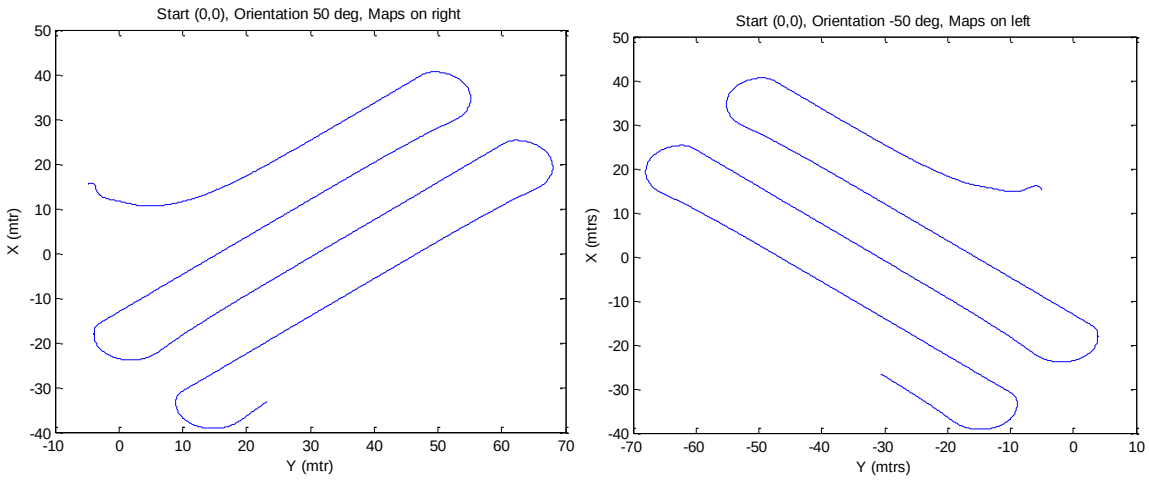

Figure 3.16: Simulation result for two different conditions. (a) Start (0,0), Orientation 50 deg, Maps on right, (b) Start (0,0), Orientation -50 deg, Maps on left

The controller is tested on the boat in real world environment. Figure 3.17 shows the performance of the boat at different orientation on a calm day. The red line shows an actual path followed by the boat and the blue line is the desired path for the boat. Mapping region is defined by green box. In each case the boat starts at different position and different heading. It then moves towards the line and then follows the line. For north run(a) and east run(b) the spacing between the paths is 20 meters and for north-west run the spacing is 10 meters. Thus various test conditions are tried and the controller is tuned for the optimum performance within operating range of 10-30 meters spacing. The Mow-the-Lawn controller performance is measured by measuring root mean square error between desired path and actual path within the mapping region. Figure 3.18 shows cross-track error for north run over the complete run. The green portion of the plots

depicts the error in mapping region. The rms error in mapping region for particular operation was 0.534 meters which is well within the desired specs.

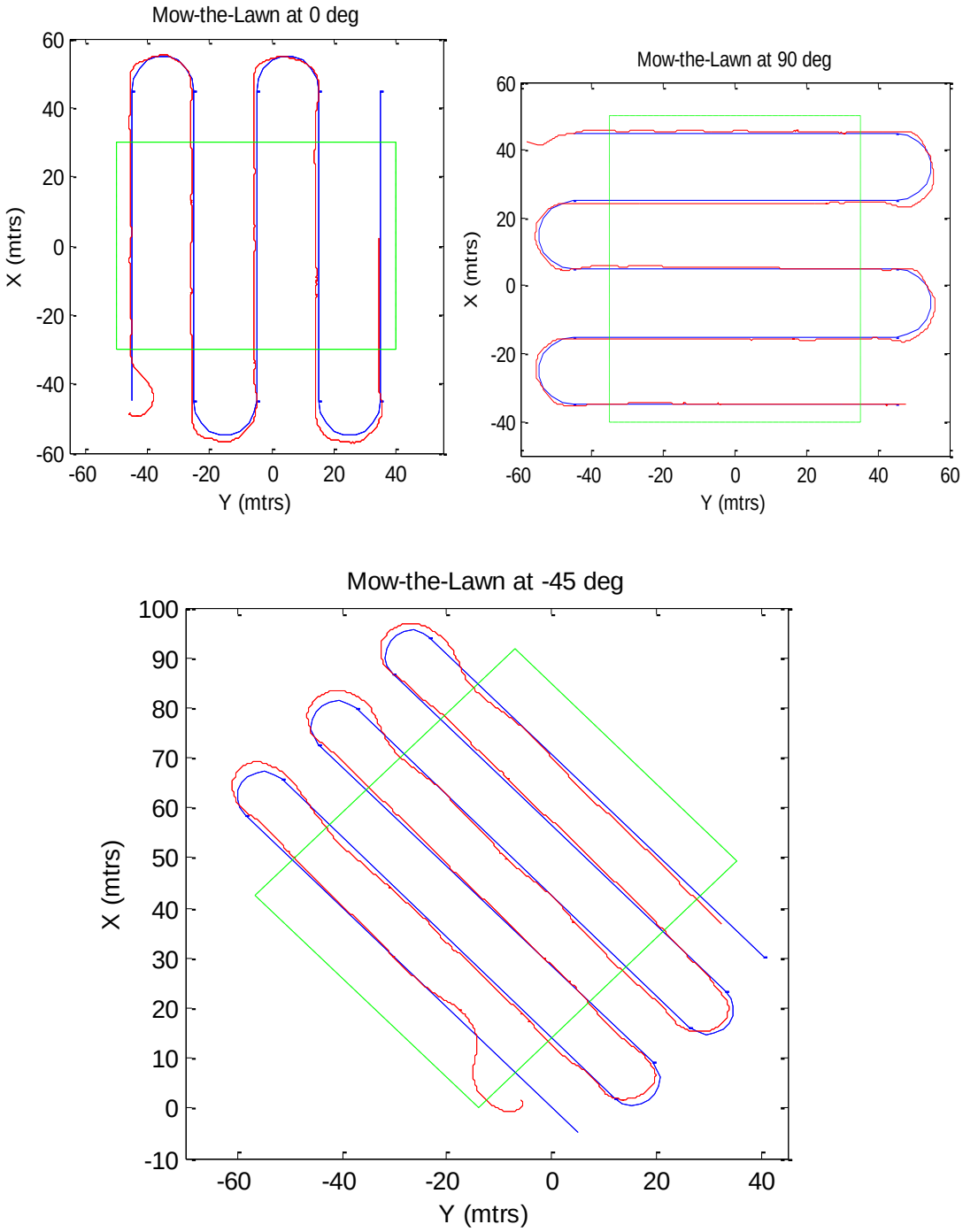

Figure 3.17: Real world test results for Mow-the-Lawn pattern of SWATH. (a) Lawncut in north direction.[37] (b) Lawncut in east direction. (c) Lawncut in north-west direction

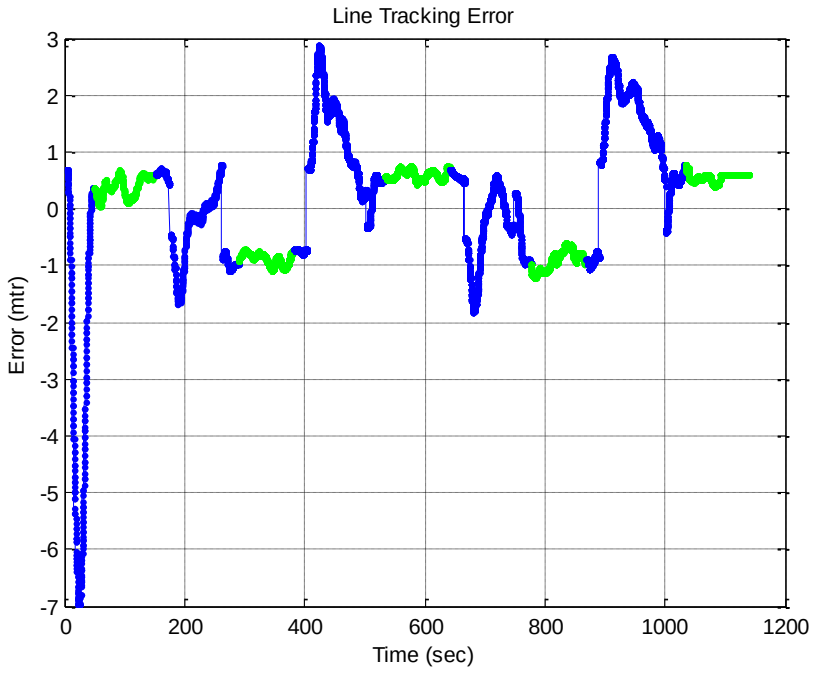

Figure 3.18: Time history of cross-track error during the mapping operation shown in 3.16(a). The green portion is error in mapping region [37]

The normal mapping conditions are not always calm. There is a wind and current which affects a normal path following of the both. These disturbances can move the boat along the path and affect the mapping performance. Thus to cope up with that a feed forward controller is developed, which measures the force acting on boat because of any disturbance and inputs the command accordingly to negate it.

3.6 Feed-Forward Dynamic Control Strategy

The strategy used by this controller was to sense and estimate disturbances and to adjust the control output to negate them. To explore feed-forward capability, this work focused on wind drag, which was prevalent in the reservoir where much of the testing for this research program occurred. In general, the drag force due to either the wind or the current is calculated with following equation

$$F_D = \frac{1}{2}\, c_d\, \rho\, \vartheta^2\, A \tag{3.24}$$

Where, F_D is the drag force, c_d is a drag coefficient, ρ is the mass density of fluid, ϑ is velocity of the biat relative to the fluid, and A is a reference area.

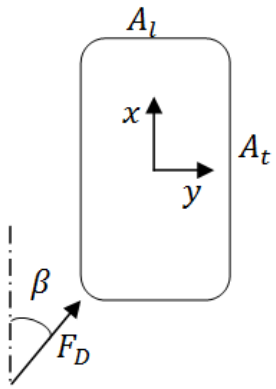

Figure 3.19: Effective area explanation. Force F_D acting on boat at an angle β with A_l as longitudinal area and A_t as transverse area.

To estimate the drag force, the effective area was calculated as a function of the relative wind direction. As shown in Figure 3.19, if F_D is acting on boat at an angle β with respect to boat frame, the boat's longitudinal area is A_l, and the boat's transverse area is A_t, then the effective area is measured as

$$A_{eff} = A_l \cos\beta + A_t \sin\beta \tag{3.25}$$

In practice, given that all terms other than speed and area are constants, the drag force computation was simplified to:

$$F_D = k_d \, A_{eff} \, \vartheta^2 \tag{3.26}$$

Where, k_d was empirically tuned in the field through a procedure that nulled the effect of the disturbance force. Given this, the disturbance speed and direction was measured in real-time such that an estimate of the disturbance force could be made.

Given a disturbance estimate, the controller summed the cross-track control force command with the negative of the estimated disturbance force in order to compute an overall control command, as shown in Figure 3.20.

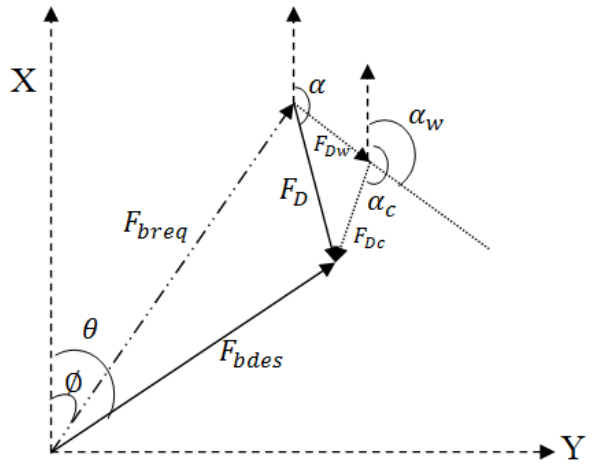

Figure 3.20: Force vector diagram for force analysis

From the Figure 3.20, "F_{bdes}" is the cross-track correction force, and "F_D" is the resultant disturbance force caused by water current "F_{Dc}" and wind force "F_{Dw}" acting at an angle "α". To provide the cross-track correction while also compensating for the disturbance force, the boat is given a control command of "F_{breq}". All these forces measured in path frame. The mathematical representation for the calculation is as follows

$$\overrightarrow{F_D} = \overrightarrow{F_{Dw}} + \overrightarrow{F_{Dc}} \tag{3.27}$$

$$\overrightarrow{F_{breq}} = \overrightarrow{F_{bdes}} - \overrightarrow{F_D} \tag{3.28}$$

$$\emptyset = \tan^{-1}\left(\frac{F_{breqy}}{F_{breqx}}\right) \tag{3.29}$$

$$F_{delta} = F_{breq} - F_{bdes} \tag{3.30}$$

$$\theta_{delta} = \emptyset - \theta \tag{3.31}$$

The values "F_{delta}" and "θ_{delta}" are provided to the controller by the feed forward loop. The developed controller measures the adjustment required for the forward propulsive force and the heading and add these to the nominal values to be used due solely to correcting cross-track error. The controller can be depicted as shown in Figure 3.21.

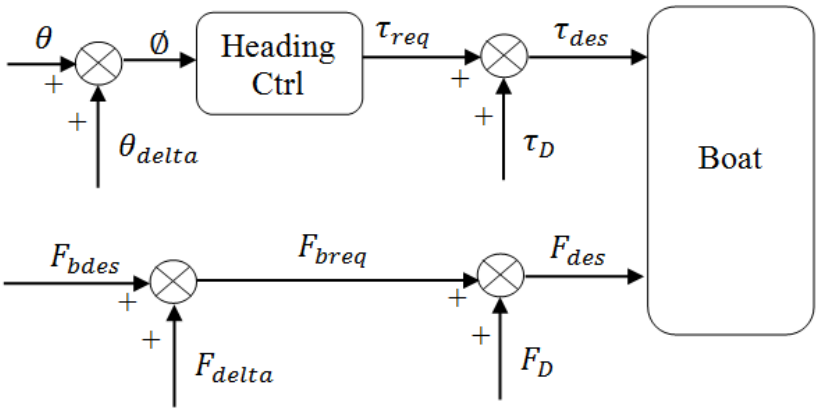

Figure 3.21: Feed Forward control block

3.6.1 Simulation results

The controller tested in simulation addressed both wind and current. Figure 3.22 shows the data for one of the multiple test cases. In this case, a constant wind of velocity 5 MPH is applied in the North direction and constant current of velocity of 10 MPH is applied in North-East direction. The blue line the desired path and the red line is the actual path. From the figure, it is clear that, without the feed-forward controller, the path has appreciable cross-track error, whereas with the feed-forward controller the controller corrects the boat to overcome the disturbance.

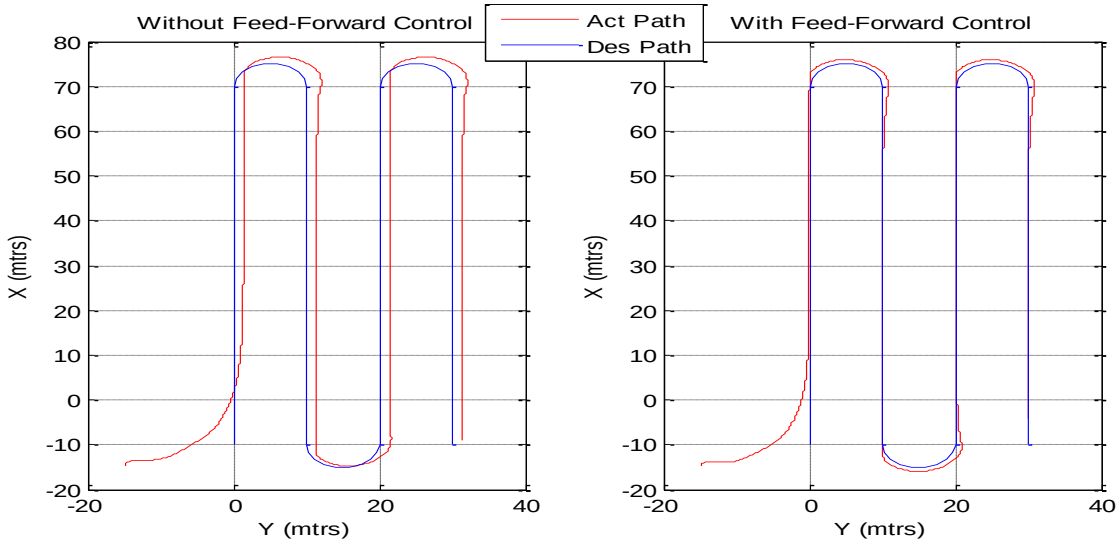

Figure 3.22: Feed-Forward controller simulation result showing Mow-the-Lawn with North wind and North-East current.

Figure 3.23 shows time history data for velocity and cross-track error. As the current was acting at 45 deg to the boat, the boat naturally tends to move faster in the North direction and its speed reduces when traveling in the South direction as current opposes the motion. The feed-forward controller compensates for this increase and decrease of the speed. The controller also corrects the cross-track error.

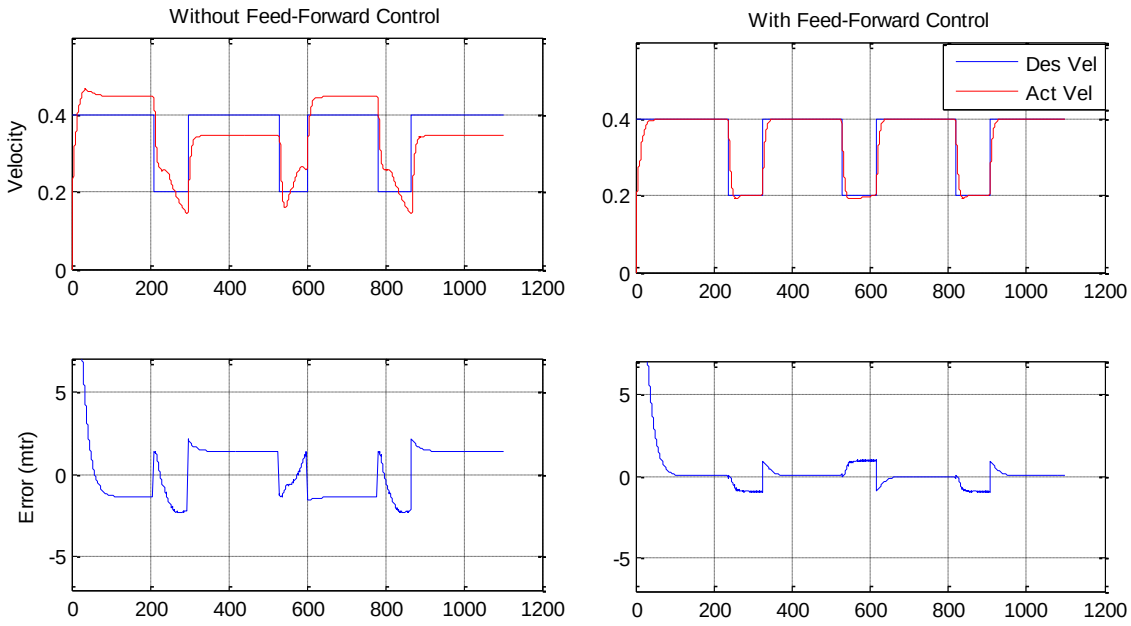

Figure 3.23: Velocity response in simulation is displayed in first plots. The cross-track error performance for the run is shown in second plot

3.6.2 Real world test results

For the real testing, only wind disturbances were addressed given that the feed-forward control option was only an exploratory element of this work. Wind disturbances were selected over current disturbances given the relative ease of measuring relative wind speed and direction.

A wind sensor as mounted on SWATH to measure the wind speed and direction with respect to the boat. This data was collected by an Arduino Uno microcontroller and transferred to the off-shore control computer using an XBee wireless communication link. Once received by the off-shore computer, this information was used to generate disturbance rejection values. An external wind sensor was also placed on shore to verify

the readings of the sensor on the boat. Figure 3.24 shows SWATH with the wind sensor during one of the operations. The tests were done in relatively high wind conditions in order to show control improvement with the use of the feed-forward controller.

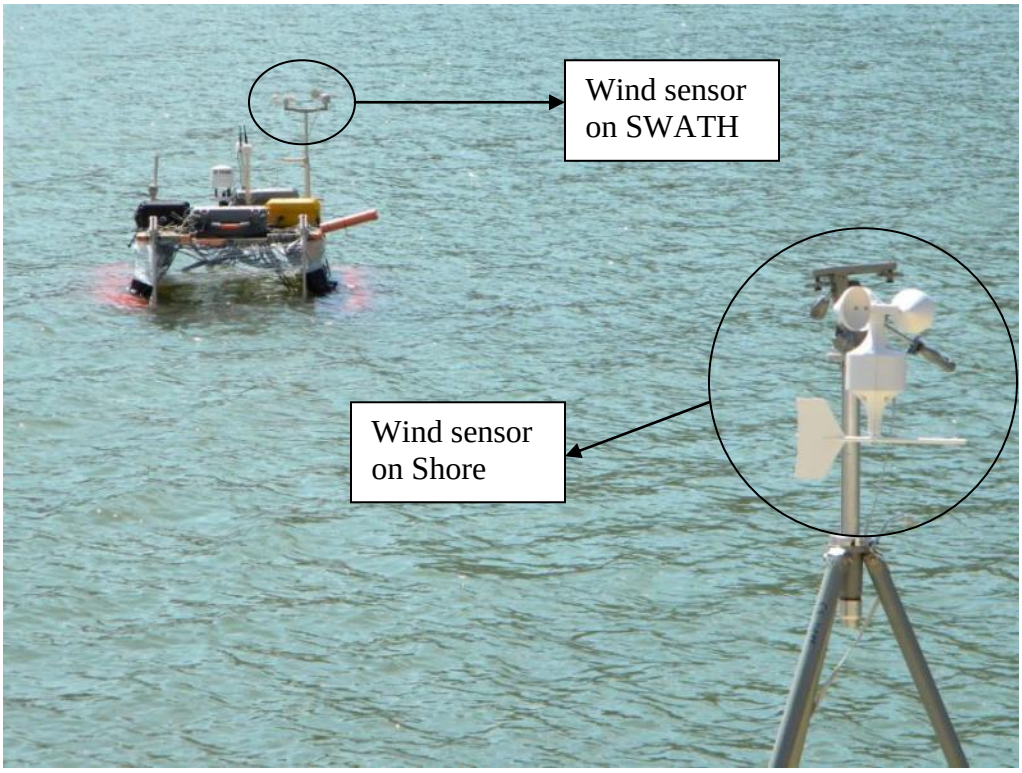

Figure 3.24: SWATH test setup for Feed-forward controller

Two experiments were run for the field tests. In the first, the boat traveled directly into and out of the wind. In the second, the boat traveled perpendicular to the wind direction.

Figure 3.25 shows the results for the first case, with the boat moving directly into and with the wind. As can be seen, in this orientation, little cross-track error occurs except during turns.

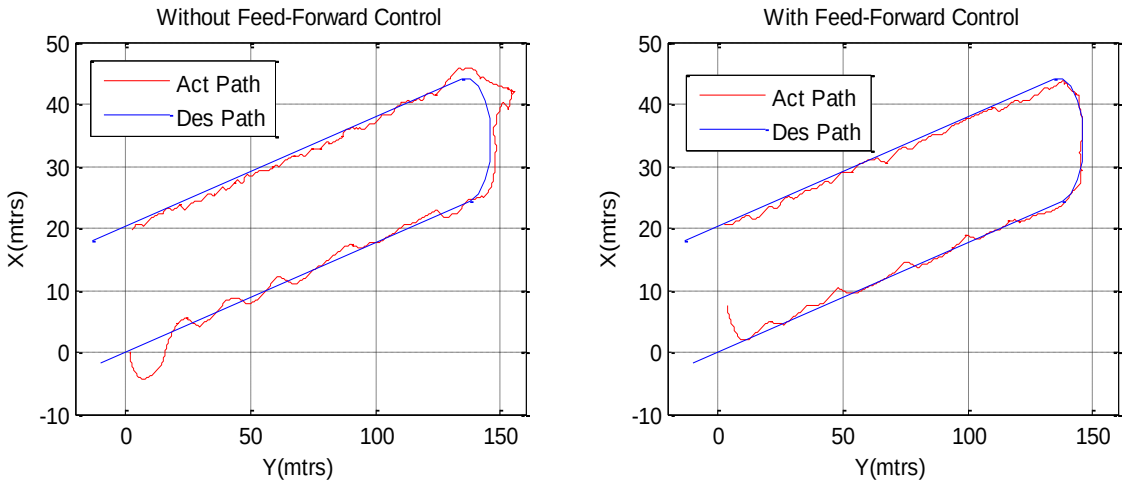

Figure 3.25: Example of path following along the wind direction (a) Without feed forward loop, (b) With feed forward loop

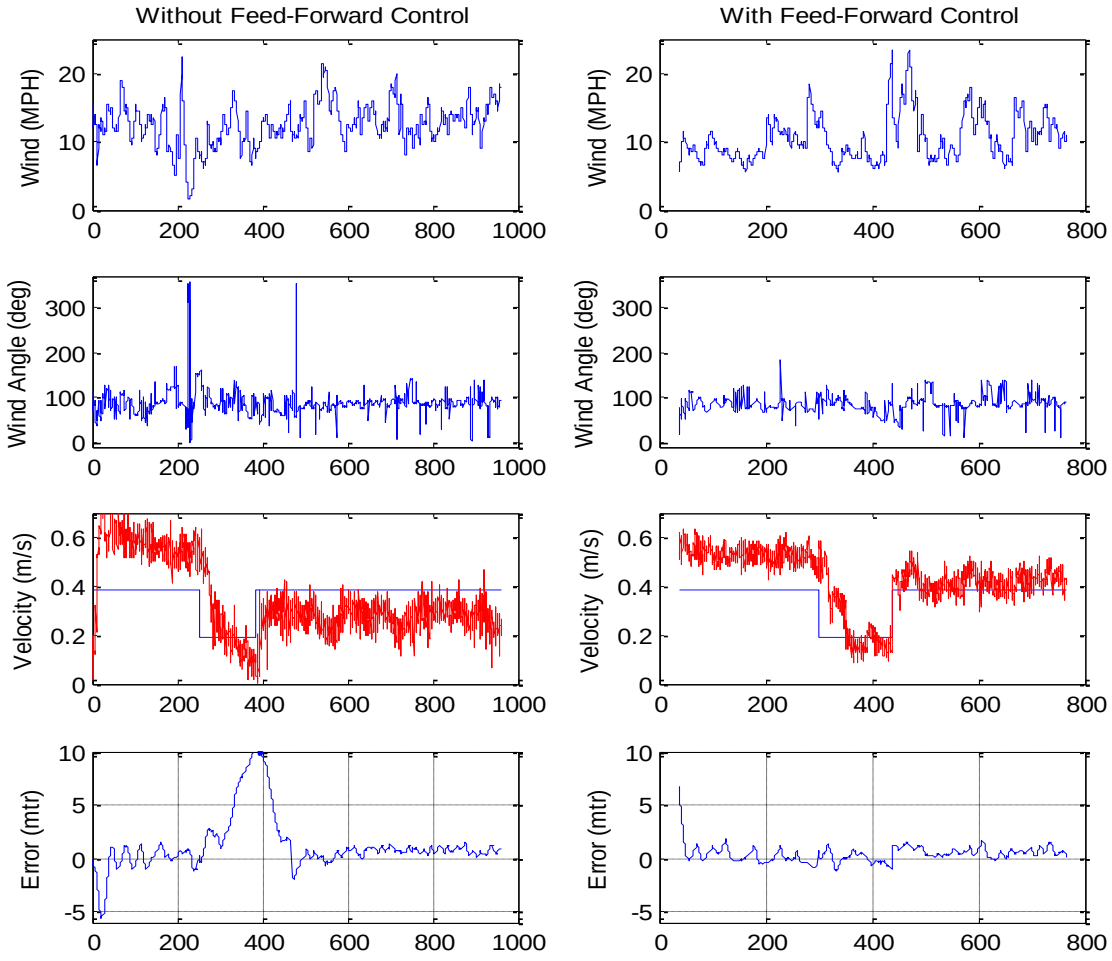

Figure 3.26: SWATH performance data for the run in figure 3.25. (a) wind speed response, (b) wind angle response, (c) Velocity response (d) cross-track error response

As expected, the main effect of the wind was a decrease of speed when moving into the wind and an increase of speed while moving with the wind.

This has adverse effect on the maps. Figure 3.26 shows the data for wind, wind direction, velocity and error. The path has an orientation of 80 degrees, and from Figure 3.26(b) the wind angle is seen to be approximately the same direction. From the velocity plot it is clear that without feed forward control, the velocity deviates more from the desired value than when the feed forward controller is enabled. The rms error for cross-track error measured for the run without feed forward control is 8.81meters vs. a rms error of 0.68 meters for the run with feed forward control.

In the second experiment, the boat travels perpendicular to the direction of the wind. Figure 3.27 shows the path followed by the boat for this condition. It is seen that, due to cross wind, the boat is pushed sideways away from its desired path, increasing cross-track error. When the feed forward control loop is applied, the boat's path-following performance is improved.

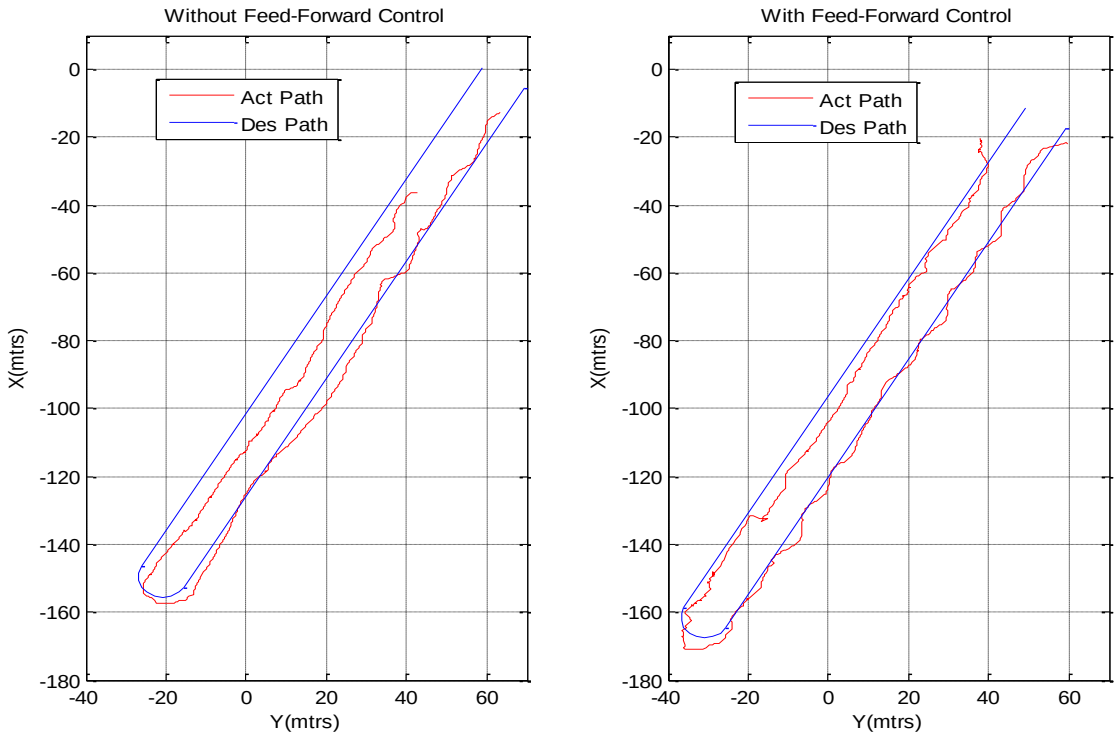

Figure 3.27: Example of path following across the wind direction (a) Without feed forward loop, (b) With feed forward loop

Figure 3.28 shows the performance data for the cross wind run. From Figure 3.27 it is seen that the path orientation is -150 degrees, and from Figure 3.28(b) the wind angle is seen to be around 100 degrees. Velocity variation is seen in Figure 3.28(c) with the blue line as desired velocity and red line as actual velocity. The cross-track error as seen in Figure 3.28(d) is higher in the run without feed forward control, with an rms error of 11.21 meters. With feed forward control implemented, the rms error is 4.29 meters.

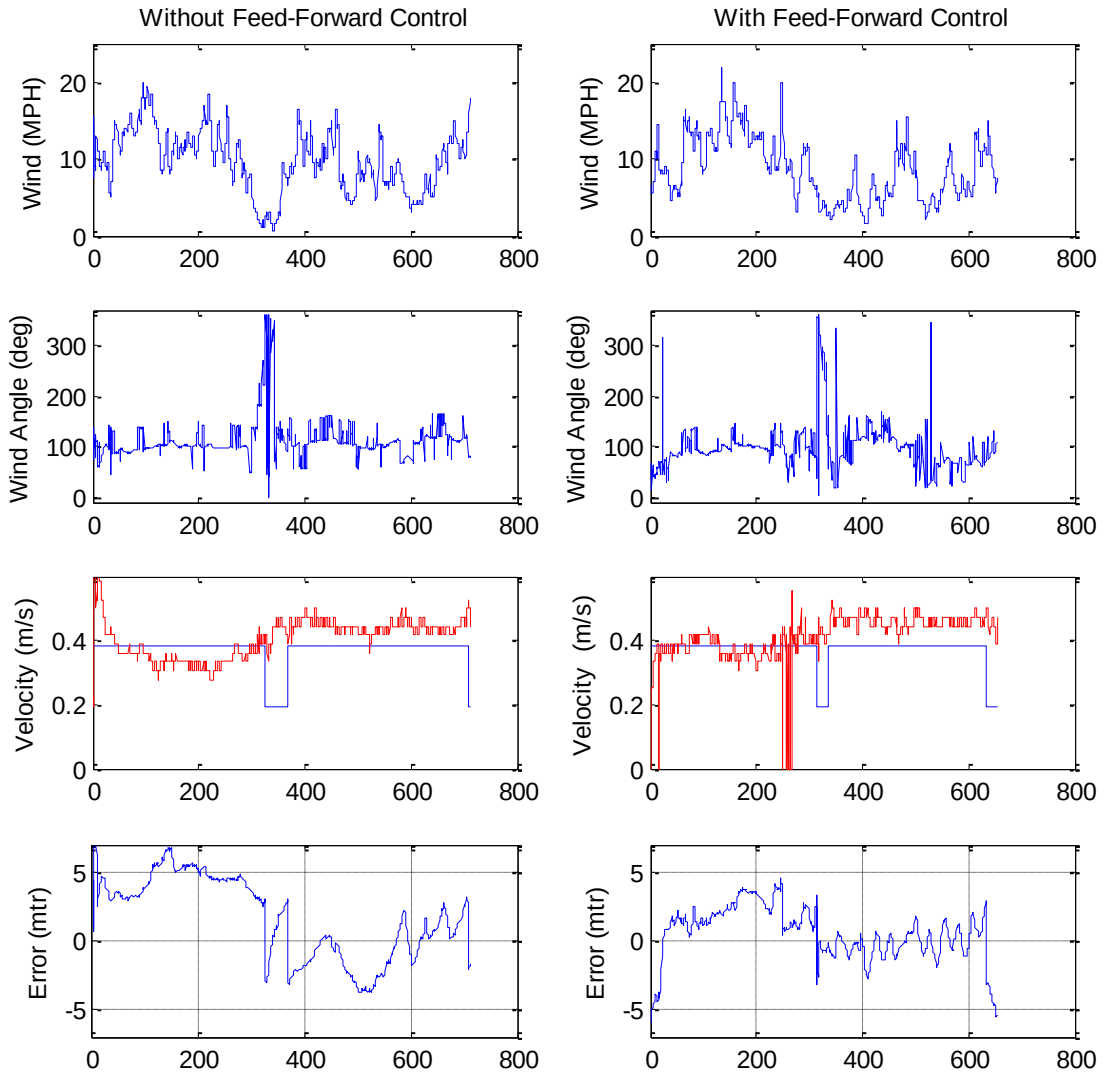

Figure 3.28: SWATH performance data for the run in figure 3.27. (a) wind speed response, (b) wind angle response, (c) Velocity response (d) cross-track error response

3.7 Navigation and control summery

In this chapter starting with basic dynamics of SWATH boat is discussed. Further the development of heading controller, line controller and circle controller are discussed. Then the sequencing to generate Mow-the-Lawn pattern is explained and simulation results are verified. The development of a higher level controller ‘Mission planning’ for end user is explained and experimental data is presented. And lastly the Feed-forward controller development with simulation results and experimental field results are shown.

Chapter 4: Canard System

A pair of differentially articulating canards is mounted on the front of SWATH as shown in Figure 4.1. The variable angle of the canards applies different pitch and roll hydrodynamic torques that can be used to help maintain level operation of the platform. Although the boat is often trimmed at the start of a deployment, pitch and roll disturbances occur due to waves, due to vessel-specific hydrodynamic torques at varying speeds, and due to centripetal torques when turning. While pitch and roll data is recorded in order to post-process sonar data, eliminating these disturbances enhances the quality of the maps and simplifies their processing. Furthermore, at high speeds, hydrodynamic torques threaten the boat's safety by severely pulling the bow of the boat close to the waterline.

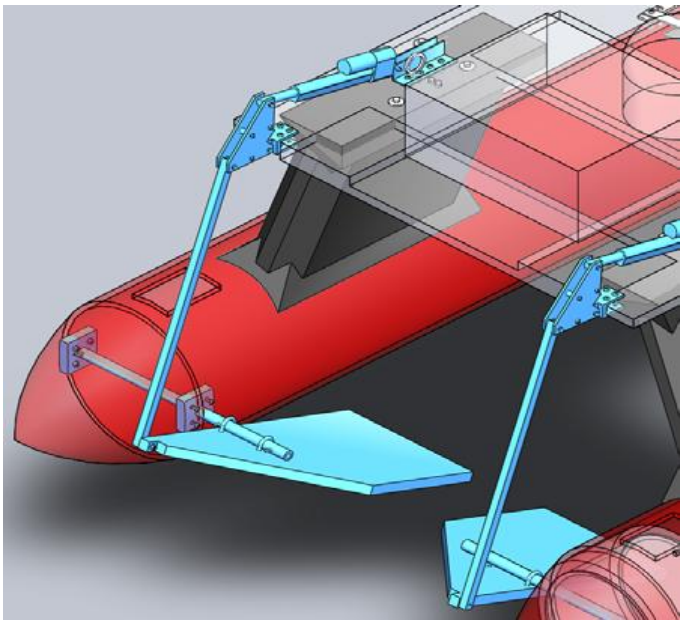

Figure 4.1: Canards mounted on front of SWATH

In principle, the canards can be used to reject these pitch and roll disturbances, thereby allowing faster boat operation, simpler map processing, operation in higher sea states, and higher quality maps. They can also account for poor trimming, allowing a

deployment to be more rapidly started. This chapter details how the canard system is used to stabilize SWATH in order to trim steady state pitch error, which varies based on the operating speed of the craft. In its current form, the canard actuators are not fast enough to address wave-generated disturbances.

4.1 System development

The canard system consists of two pinned plates that are rotated by deck-mounted linear actuators via a transmission system, shown in Figure 4.1. A CMPS10 compass reads roll and pitch inclinometer outputs and provides a sensed platform pitch estimate to an Arduino Uno microcontroller. When switched to automatic mode, the Uno computes the desired canard actuator position and, knowing the current canard angle via linear actuator feedback, provides a PWM control signal to each of two channels of an AX1500 Roboteq motor control board, which moves the actuators accordingly. The system also supports manual control of the canard positions.

The control system architecture is depicted in **Error! Reference source not ound.**. The architecture consists of an inner canard angle position control loop surrounded by a boat pitch control loop. The design of this system was established empirically, without any detailed modeling of the boat pitch dynamics or the hydrodynamic torques generated by the canards. A proportional controller was used for the canard position controller in order to achieve critically damped canard position behavior; a full PID control law was used in the boat pitch loop in order to achieve a settling time on the order of 30 sec (which is a typical minimum threshold for the amount of time the boat operates at speed prior to initiating mapping operations).

The control equation for the canards are shown below

$$\emptyset_{cdes} = k_p * [\,\theta_{bdes} - \theta_b] + k_i * \int_0^t [\,\theta_{bdes} - \theta_b] \tag{3.32}$$

$$pwm_1 = k_{c1} * [\emptyset_{cdes} - \emptyset_{c1act}] \tag{3.33}$$

$$pwm_2 = k_{c2} * [\emptyset_{cdes} - \emptyset_{c2act}] \tag{3.34}$$

$$\tau_{b1} = k_t * \emptyset_{c1act} \quad (3.35)$$

$$\tau_{b2} = k_t * \emptyset_{c2act} \quad (3.36)$$

$$\tau_b = \tau_{b1} + \tau_{b2} \quad (3.37)$$

Where, k_p and k_i are PID gains for pitch control, k_c PID gain for canards and k_t conversion factor for torques. A graphical snapshot of the Simulink controller used for field test is shown in Appendix C.

4.2 Field Testing

For experimental verification of the canard control system, the boat was tested in calm lake water over a range of different velocities. Water current and wind effects were minimal during these tests and therefore neglected.

For demonstration, the boat was improperly trimmed such that it had a pitch offset angle of 4 degrees (nose down). Thus objective of the control system was to bring the boat back to the level orientation. SWATH was operated in a straight line at constant speed in Foster City Lake as shown in Figure 4.2. The speed was increased gradually from 0.32 m/s to almost its double 0.69m/s both with and without the canard controller enabled.

Figure 4.2: SWATH operation at Foster City Lake

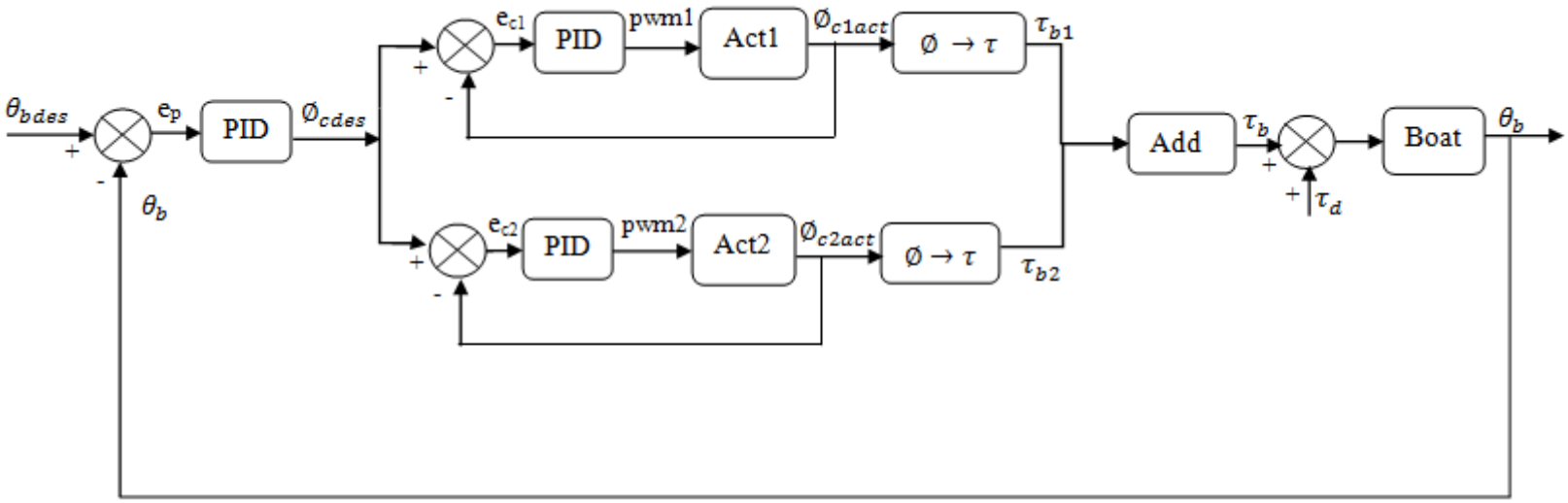

Figure 4.3: The control system architecture with inner canard angel position control loop, where, $\theta_b$is pitch angle of boat, e_p is pitch error, $\emptyset_c$ is angle of canards, $\tau_b$is torque acting on boat, $\tau_d$is disturbance torque, Act1 / Act2 are actuators, e_c is error in canard position, τ_{b1} and τ_{b2} are torque generated by canards.

Test results are shown in Figure 4.4, with each plot showing the measured pitch angle for trails at a given forward speed, both with and without the canard system enabled. From the figure, it can be seen that, for all speeds, boat pitch stayed at approximately 3-4 degrees or more without the canard system. With the canard system turned on, however, pitch was successfully trimmed to a zero pitch orientation for nearly all operating speeds; this occurred with a transient response of about 30 seconds, which is quick enough to stabilize the boat at the beginning of a mapping session before it gets to its region of interest. It is worth noting that prior to the use of the canards, the boat's speed during mapping operations was limited to a speed in the 0.3m/s to 0.4m/s range because of pitching concern. This data shows that the speed can be nearly doubled without pitching concern for faster, more efficient mapping with no sacrifice in quality. Figure 4.5 shows the RMS error in pitch after the boat settles for different velocities. It is clear that with active canards the error is less than 1deg for almost all the cases except 0.32m/s.

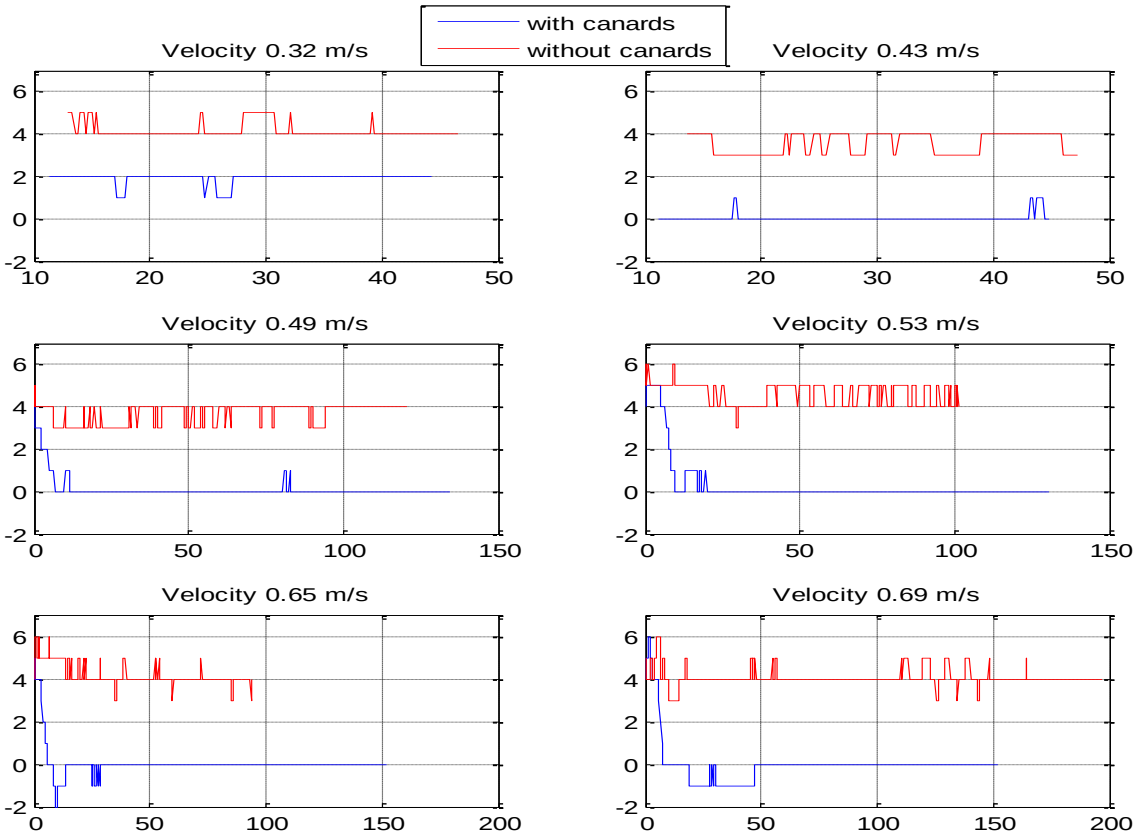

Figure 4.4: Boat response with and without canards at different speeds

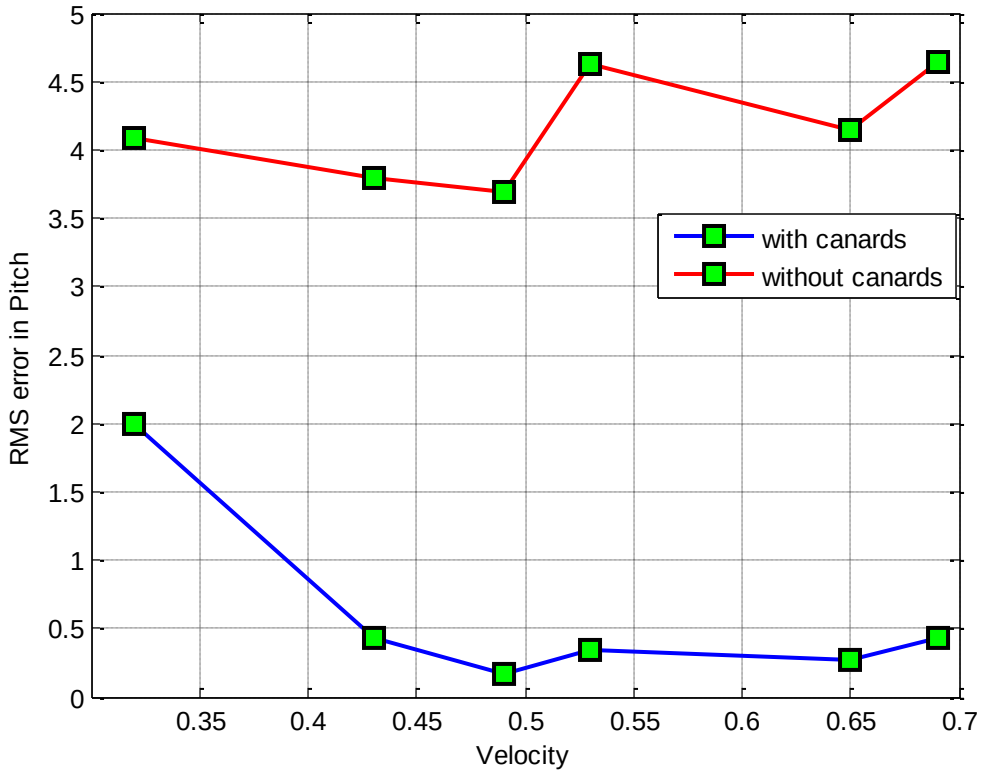

Figure 4.5: RMS error plot for all the velocities comparing data for with and without canards

From above data, it is seen that for a 0.32m/s velocity the pitch is not fully trimmed, settling at an error of about 2 degrees. This is because the hydrodynamic torque that acts on boat is not only a function of canard angle but also of the velocity of the boat. As it turns out, for operation at 0.32 m/s, the controller moves the canards to the maximum value of 30 degrees, thereby saturating the system and preventing level operation at this speed. It is possible to increase the range of the canards such that they move over a range of up to +/- 65 degrees. However, with such a wider range of motion, instability is possible at the higher operating speeds; an example of this is shown in Figure 4.6. Since we wish to operate the boat during mapping operations at the higher speeds, the canard operating range and the control gains were set to meet control specifications at those speeds such that the inability to level the boat at 0.32 m/s is inconsequential.

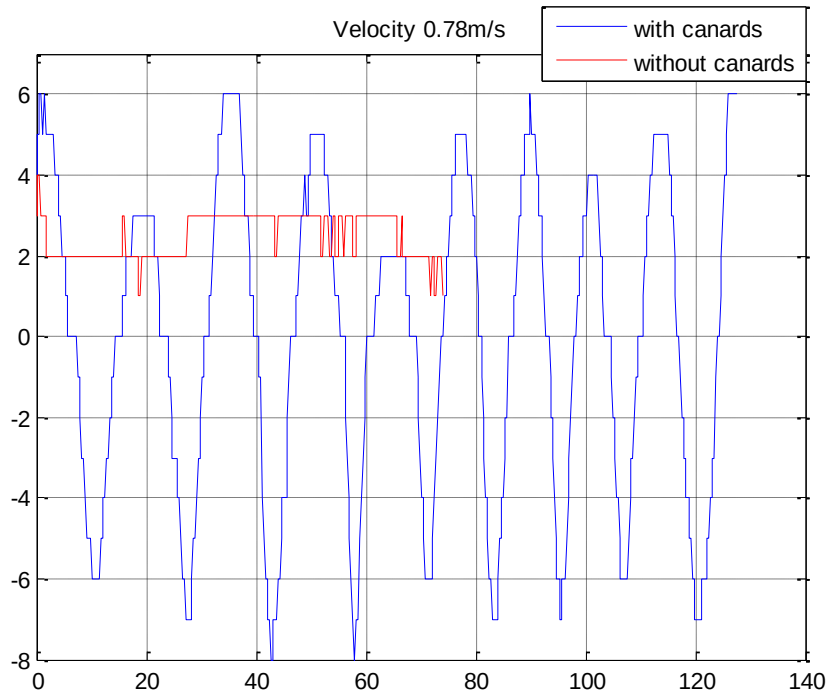

Figure 4.6: Unstable response of the boat - at 0.78m/s speed and with +/- 30 degree range of canards

4.3 Summary of Canards System

This chapter reviewed the control of the boat's canard system, describing the design of the controller and presenting experimental results from field testing. These results show that the system properly functions in order to trim boat pitch for steady state hydrodynamic disturbances. This allows the boat to be confidently operated at nearly twice its standard operating speed, which translates into the production of maps at nearly twice the speed without any sacrifice of performance.

Chapter 5: Bathymetric Mapping

The SWATH boat's main function is to create bathymetric maps. It is capable of doing this in an automated manner for durations on the order of hours and in very shallow water on the order of less than a meter. These characteristics provide niche value for the system.

During operation, data is collected from a number of sensors in order to effectively generate maps. These sensors, shown in Figure 5.1, include an Imagenix 837 "DeltaT" multibeam imaging sonar sensor, a high precision marine-grade Trimble GPS unit, a Crossbow Attitude Heading Reference Sensor and a Teledyne Heave sensor. This chapter reviews how data from these sensors is collected and filtered in order to generate complete bathymetric maps.

Figure 5.1: SWATH mapping sensor suit. (a) Imagenix 837 "DeltaT" multibeam imaging sonar sensor, (b) Trimble GPS unit, (c) Crossbow Attitude Heading Reference Sensor, (d) Teledyne Heave sensor.

5.1 Mapping data collection

Under a different, ongoing capstone project by SCU student Vivek Reddy [41], a suite of software programs were developed to collect data from each sensor such that it can all be processed by the MBSystem mapping software. Separate executable programs collect and log data from each sensor through RS232 connections or via Ethernet for the sonar. This data is recorded on the on-board computer in different files for each sensor. Every sensor has a different frequency for streaming the data; therefore, each data point is time

stamped with respect to computer. Once all these files are collected once operation is completed, another program is used in order to merge the files, with data organized in chronological order.

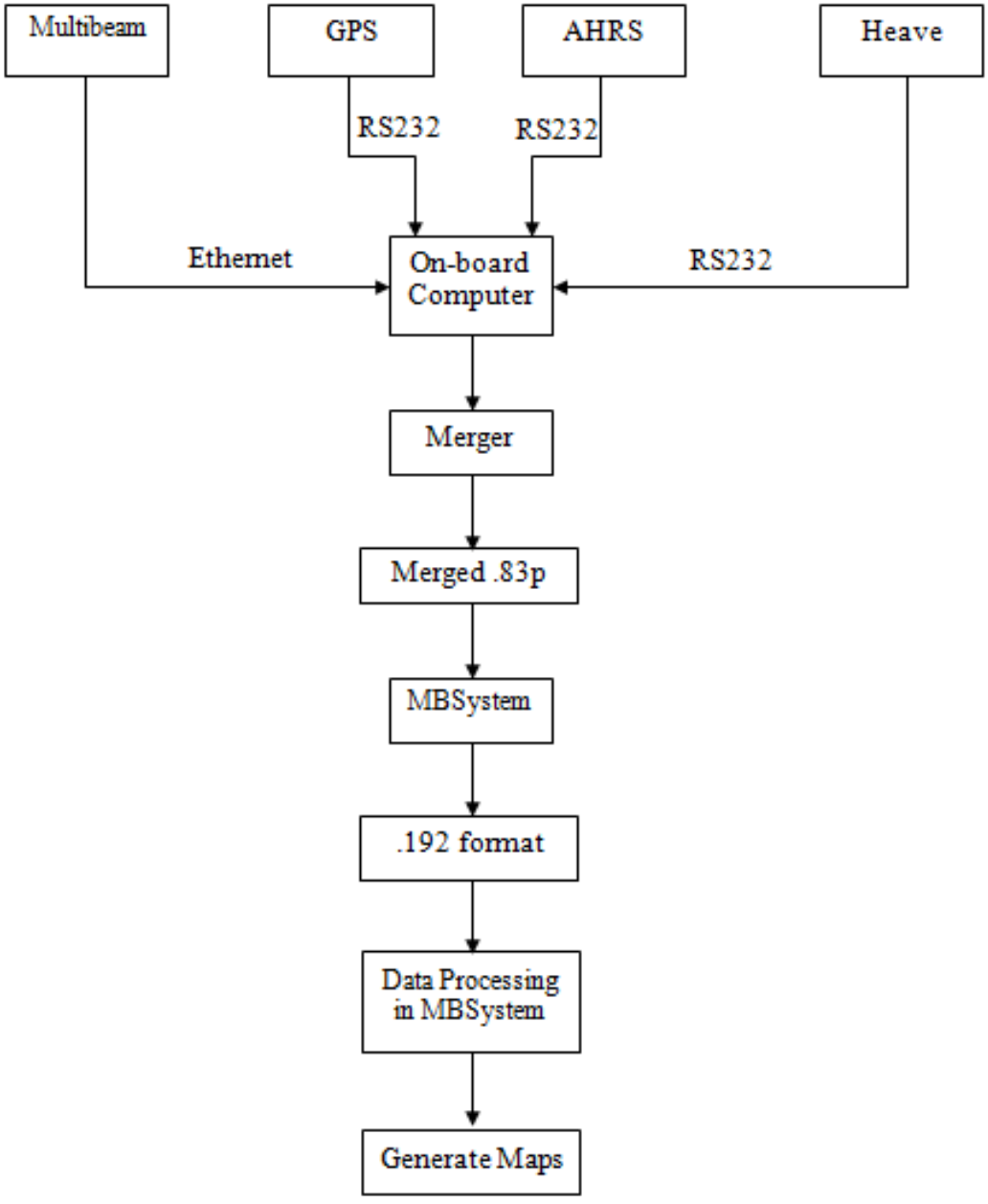

Figure 5.2: SWATH data collection Flow-chart

This merge creates one consolidated file, formatted and saved as a ".83p" file, which is a file standard for the MBSystem software, which is a Linux based open source software environment used to create the maps. The flowchart for this overall process is shown in Figure 5.2.

5.2 Post-processing in MBSystem

The .83p files are converted to .192 files which is a standard format used by MBSystem. This .192 file can be viewed in the MBSystem GUI. The various functions in MBSystem allow the collected data to be filtered and manually edited in order to remove noise and sonar artifacts. Figure 5.3 shows examples of noise from a multibeam sonar. The center rise is the effect of multiple reflections of the center beam from the bottom. Sometimes random reflections are also seen due to bubbles or floating objects such as the weeds. The data points which are not normal for the terrain are deleted to get the correct map.

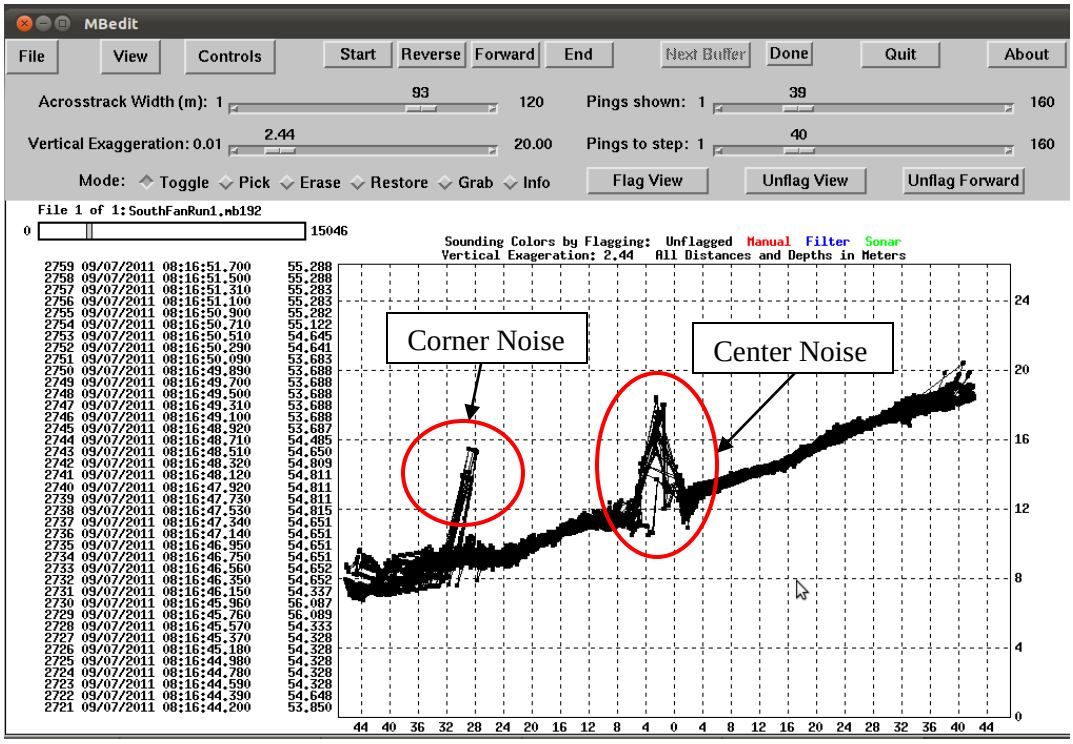

Figure 5.3: Example of the sonar noise. This image is a GUI window of MBEDIT function in MBSystem to clear the sonar noise

Sometimes with this noise, a constant roll or pitch offset is also seen in the data. MBSysem roll-bias / pitch-bias function is used to fix this. Figure 5.4(a) shows the map with raw data. The noise and the roll offset is seen in the figure. Figure 5.4(b) is the map that results after removing the roll offset.

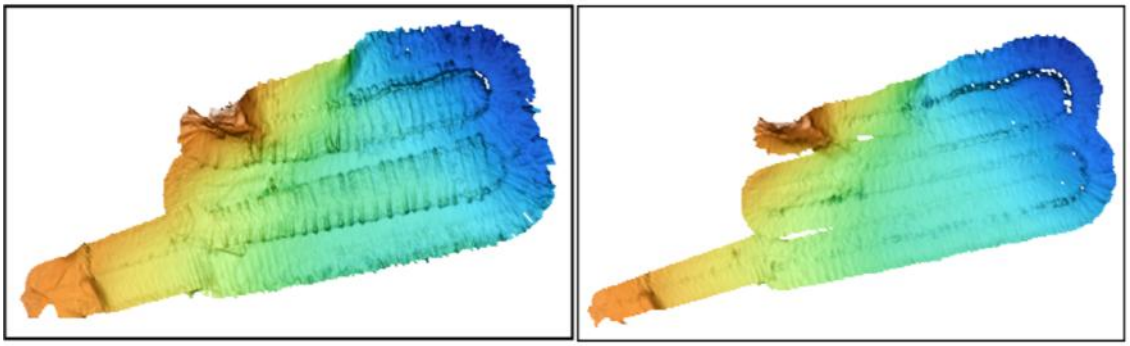

Figure 5.4 (a) Map before cleaning the data (b) Map after cleaning the data.

Noisy GPS data can result due to issues such as multipath, and such noise leads to problems when generating a map. The variation in GPS path can be seen by the MBSystem tool. MBSystem provides an interpolation function for GPS data points in order to smooth data. An example of a noisy path and its filtered result is shown in Figure 5.5 and Figure 5.6.

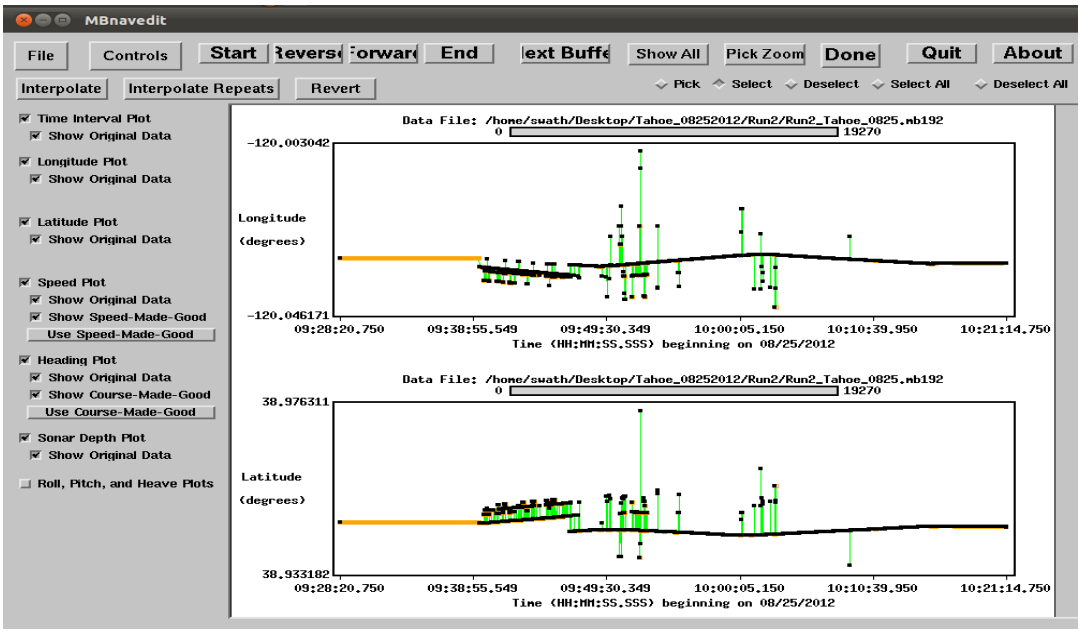

Figure 5.5: GPS noise as seen in MBSystem GUI function

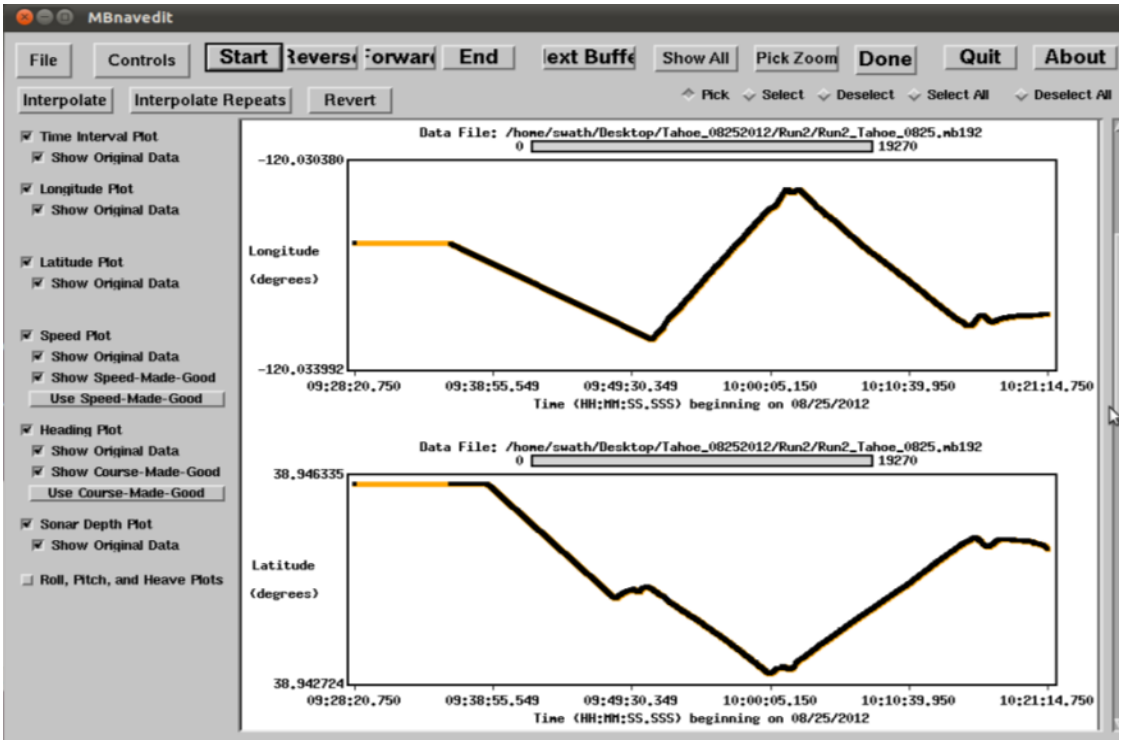

Figure 5.6: GPS data after interpolation as seen in MBSystem GUI function

5.3 Mapping Characterization

To characterize mapping precision, a standard procedure developed by MBARI [41] was used. A specific region is mapped multiple times using different path orientations, and the spatial difference between the depths from both maps is analyzed. A test of this type was carried out for SWATH at Stevens Creek Reservoir in Cupertino, CA. The test conditions were ideal with no wind, current or waves. The approximate depth of the reservoir is about 20 meters and the mapping speed was 1.6km/hr. The maps generated with this in different orientations were overlaid, and the result is shown in Figure 5.7(b). Figure 5.7(a) shows the error map, showing the depth differences at any point, for the overlapped region of the two runs. Figure 5.7(c) is a frequency histogram of errors. This data proves the bathymetric repeatability of 0.268m at one standard deviation for given depth and conditions. Maximum deviation is shown by red circles in the figures; these locations correspond to the locations of maximum gradient. This type of error is due primarily to the variation in the position data of the boat.

Bathymetric repeatability performance is typically presented as a percentage of the depth. From the above tests, a repeatability of 1.4% of the depth is achieved, which is an excellent result compared to an industry target of 5%. Such good results are definitely due to the good weather conditions, but it validates the level of precision that can be achieved.

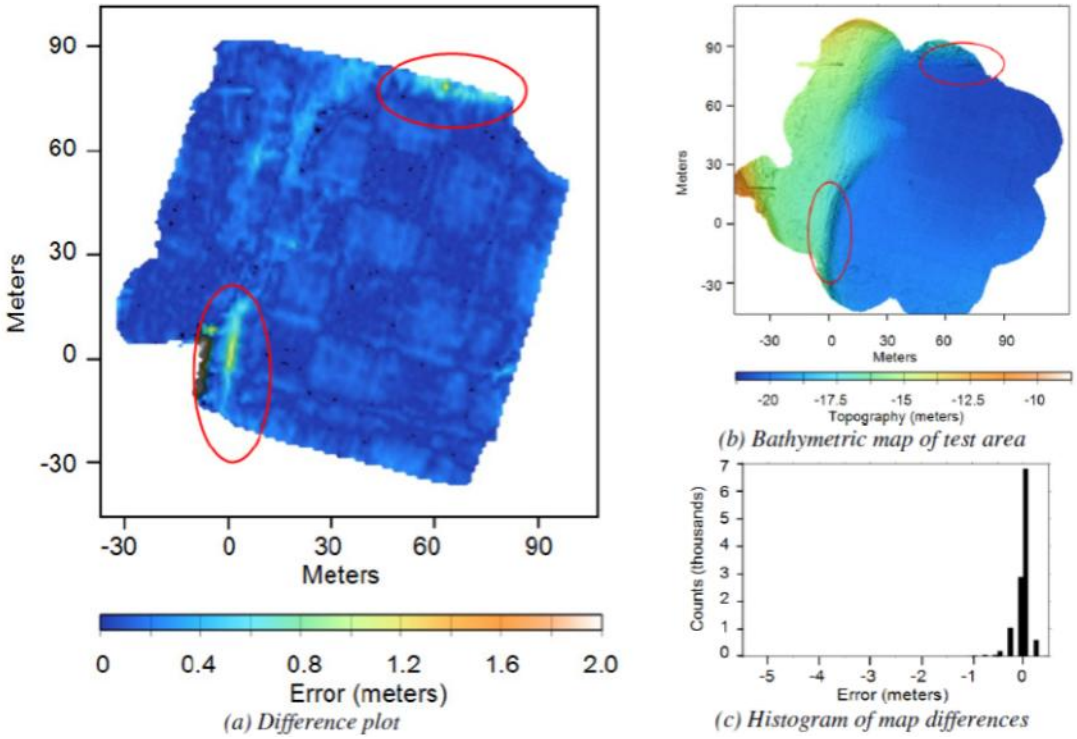

Figure 5.7: Precision test results. (a) Error Plot – difference in depth over the same region. (b) Actual overlaid map for two runs in different orientation. (c) Histogram of the difference of the depths [37].

5.4 Field Operations

The SWATH boat has been operative in the field for more than 3 years, with numerous improvements made over that time. In Fall 2009, SWATH performed its first scientific mapping operation in Lake Tahoe, California. Since that time, it has been used for many large scale mapping operations in Lake Tahoe and Stevens Creek Reservoir in Cupertino, California. Other than these, SWATH is been operative for development and test purpose

in several Northern California locations to include Elkhorn Slough in Moss Landing, San Francisco Bay, and number of additional lakes, reservoirs and estuaries. These missions are outcomes of collaboration with many government agencies and scientists.

For the 2009 Lake Tahoe mission, the team worked with marine geologists from the USGS and the University of Nevada, Reno (UNR). In previous missions with the same team, the team had used the SCU Triton ROV for underwater exploration and had found evidence of tsunami waves in the form of large scale boulder ridges along the Tahoe shelf at the North end of the Lake [42]. For the Fall 2009 mapping mission, SWATH followed the ROV path to map sections of the boulders ridge. Figure 5.8 shows a perspective view of a portion of the ridge. Average depths in the region matched with USGS LIDAR bathymetry collected in 2000.

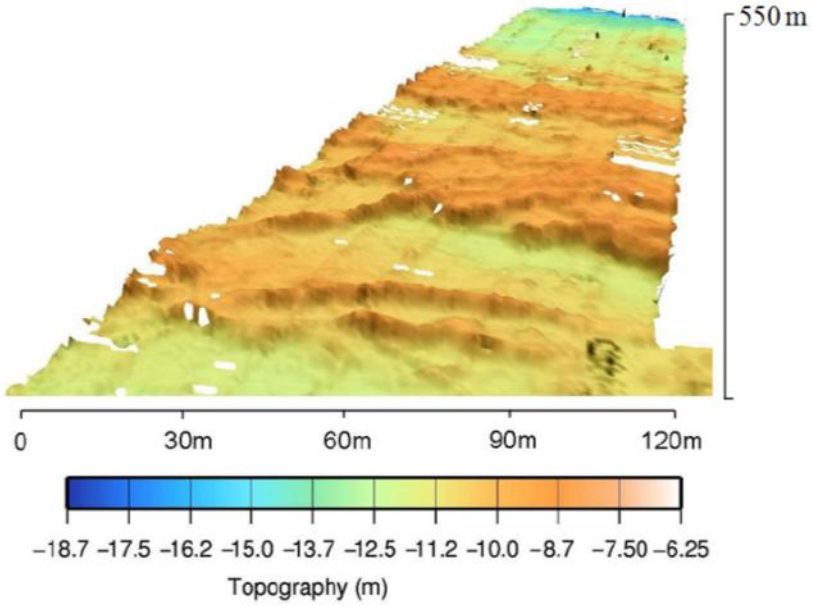

Figure 5.8: Perspective view of the boulder ridge in Lake Tahoe during the first mapping operation of SWATH in Fall 2009 [37]

The Santa Clara County Parks Office has been helpful in supporting the testing and development of SWATH by allowing its use in the Stevens Creek Reservoir in Cupertino. Figure 5.9 is the overlaid bathymetric map of the reservoir on an overhead photo from Google maps. This composite map is generated by various small operations

carried out throughout 2011. The map clearly shows the man-made structure of the reservoir. The reservoir is used for SWATH development to include the navigation and bathymetric testing discussed earlier.

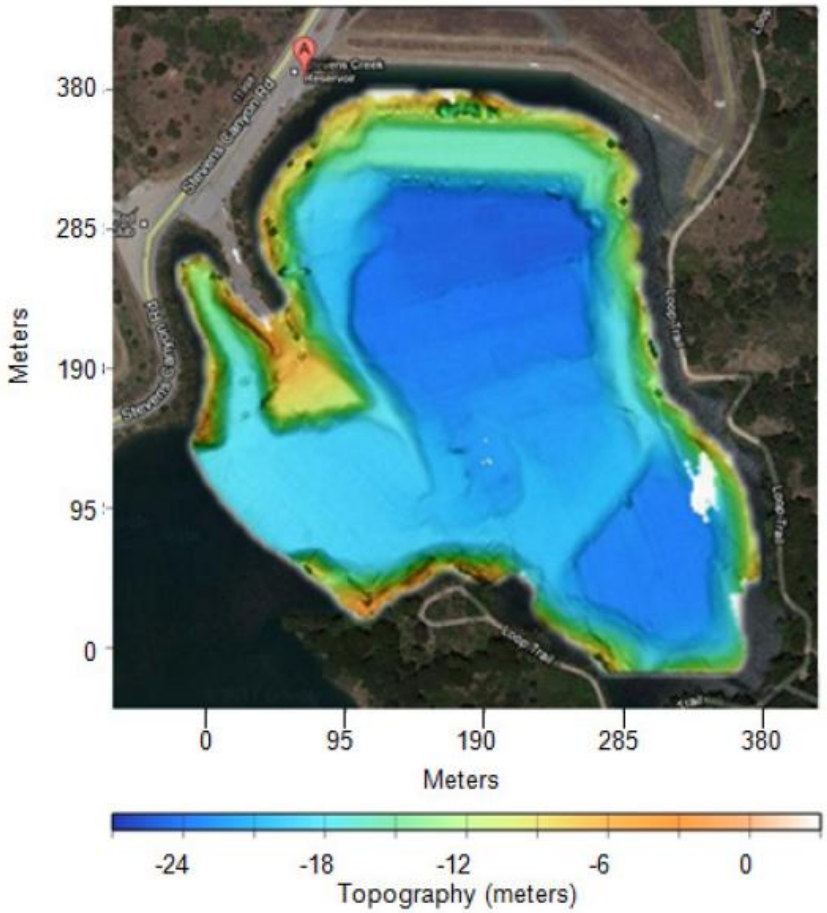

Figure 5.9: Composite bathymetric map of Stevens Creek Reservoir overlaid on Google Map during the mapping operations in 2011 [37]

In 2011, the team worked with USGS scientists in Emerald Bay in Lake Tahoe in order to generate several bathymetric maps. Figure 5.10 presents the mapped portion of Emerald Bay overlaid on an overhead Google map image. USGS geologists working in that area found previously found a number of geologically-interesting features, such as faults, on the land around Emerald Bay. The mission was mainly carried out to observe how these features are formed underwater. The overall map was generated during two missions of 5-7 days each.

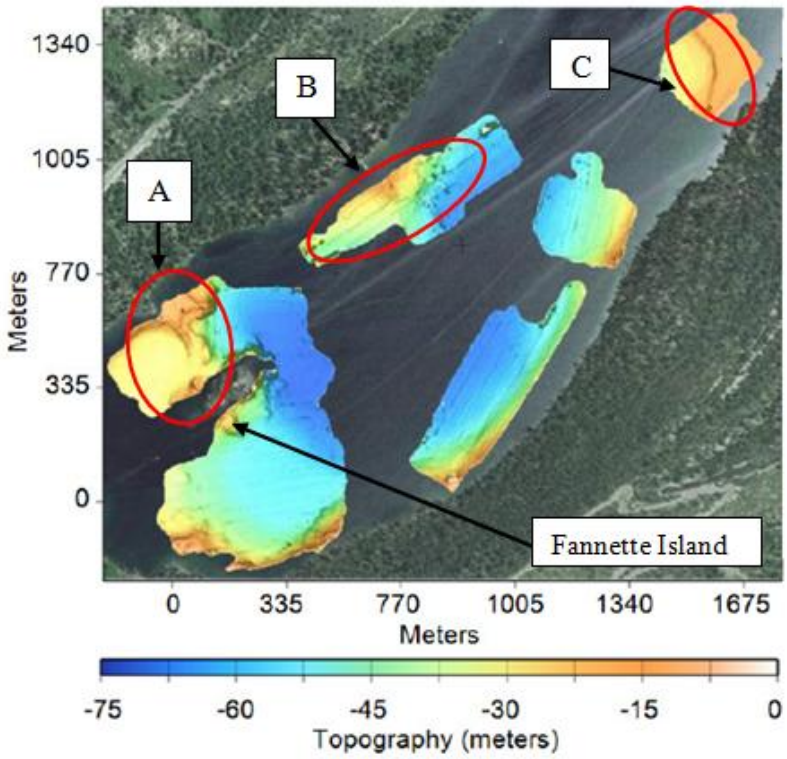

Figure 5.10: Composite bathymetric map of Emrald Bay in lake Tahoe overlaid on Google Map during the mapping operations in 2011 [37].

The area around Fannette Island in Emerald bay was of main interest to scientists. At point A, there is a dramatic drop of about 20 meters which seems to be the fault line. At point B, there was landslide that can be seen to extend into the bay. At point C another ridge was found. These maps were used as a reference to select new dive sites for the Triton ROV.

With these main missions SWATH is actively participating in many small missions and generating maps for various organizations at various locations. It is also providing information for different RSL robots like Triton and gradient climbing kayaks[43,44].

Chapter 6: Conclusion

The objective of this research project was to develop improved navigation and control capabilities for the SCU SWATH vehicle in order to improve its ability to cost-effectively perform bathymetric operations. This included the refinement of the vehicle's path-following controller and the creation of high-level path generation interfaces to generate the Mow-the-Lawn patterns used for bathymetric mapping. Further it also included experimentation with a dynamic feed-forward controller to counteract wind disturbances and also with a canard controller to trim velocity-induced steady-state vehicle pitch errors. Elements of these controllers were integrated into the vehicle's operational control software and were used in multiple science field operations. The result is improved vehicle control performance that directly translates into improved map quality, faster map generation, and system ease of use.

Figure 6.1: SWATH operating in South Lake Tahoe

6.1 Summary of work

In performing this research and development program, a number of activities were conducted in order to improve the performance of the SWATH vehicle.

To begin, the SWATH boat was dynamically tested and experimental results were used to generate a simple system model. Specifically, the relationships between velocity, thruster PWM setting, and thruster force were experimentally determined. These were used in a simulation environment in order to improve a path following controller, using an inner heading control loop. With path-following implemented, a high-level navigation controller was developed; this controller sequences through a series of path segments that are provided to the path controller for real-time operation. Furthermore, an interface and a specification model were developed in order to create "mow-the-lawn" path segment. This consolidated suite of controllers and tools were rigorously tested in the field under various test conditions and with different path orientations, specification frames of reference, different operational quadrants within these frames, different path parameters and starting points, etc. In a field test under calm conditions, the rms error in path-following capability within the mapping region was 0.534 meters, a level of performance that was well within the desired specification.

To overcome disturbances like wind and water current, a feed-forward controller was developed and evaluated. Both disturbance types were addressed in simulation, but since this was only intended to be proof of concept work, only wind disturbances were addressed during field test. To reject wind disturbances, a new wind sensor suite was installed and integrated within the control system. The developed wind feed-forward controller was evaluated during two tests, one with the boat moving in line with the wind and the other with the boat moving across the wind. Experimental results showed improvements both in the ability to maintain the specified forward translational speed as well as to reduce cross-track errors. More work on this system is required, however, before it can be included as a standard control element in the operational SWATH system.

To improve mapping speed, a pre-existing but non-functional canard system was re-engineered. The hardware mechanism itself was modified, and a new controller was developed. Experimental field data confirms that with the use of the canards, the operating speed of the vehicle can be doubled from about 0.35 m/s to 0.7 m/s given that the canards prevent the boat from pitching too far forward at high speeds.

Given the improvements to boat navigation and control, the ability of the boat to create bathymetric maps was dramatically improved, and mapping performance was characterized. In repeatability tests performed on a calm day, the SWATH system produced maps of a specific region with a repeatability of 0.268 meters at one standard deviation for given depth and conditions. This equates to a repeatability of about 1.4% of operating depth, which is outstanding given the typical acceptable performance level is 5% of depth.

Overall, these improvements have allowed the SCU SWATH boat to be used for several scientific operations in different locations and with a well-respected external geologist over the past three years. The incorporated improvements have led to improved mapping performance, faster generation of maps, and easier use of the operations software in conducting field work.

6.2 Future work

Future plans for the navigation and control system include making it more robust. This can be done by focusing more on developing a proper system model for the SWATH boat. With an improved model, the control design process will be better equipped to address disturbances as well as cross-coupling effects, such as roll motions during turns and pitch motions during translational acceleration/deceleration. Given the cost in developing and tuning a controller in the field, it is critical for a higher fidelity model to be developed in order to explore control refinements in simulation.

Feed-forward controller was a conceptual development. With the tests it is been proved that this can be a valuable addition to the navigation and control technique. In the future, a more systematic study of the drag forces can be done. This will help developing and tuning a robust controller. Furthermore, a water current sensor should be developed

and installed in order to estimate the actual current forces on the SWATH hull. This will enable the inclusion of current feed-forward control, which will lead to improved navigation performance.

For the canard system, the goal for this research project was limited to pitch trimming. The boat rolls at it turns, which has adverse effect on the data collection. In the future, both pitch and roll controls can be activated simultaneously via differential canard actuation in order to get better results on the turns. Also the system is slow, making it appropriate only as a means of trimming steady state errors. The mechanism design should be adapted to allow higher bandwidth operation. This will allow a future team to use the canards to address higher frequency disturbances, such as wave action.

References

[1] H.S. Bailey, “The Voyage of the Challenger,” Scientific American, 1953. Reprinted in Oceanography – Some Perspectives, J.R. Moore, ed. San Francisco, CA: W.H. Freeman and Company, 1971, pp. 20-24.

[2] JJ. Irish and T.E. White, “Coastal engineering applications of high-resolution lidar bathymetry,” in Coastal Engineering, vol 35, no 1-2, 1998, pp. 47-71.

[3] R.J. Urick, Principles of underwater sound. : New York, NY: McGraw-Hill Book Company, 1983.

[4] H.K. Farr, “Multibeam bathymetric sonar: Sea beam and hydro chart,” Marine Geodesy, vol 4, no 2, 1980, pp. 77-93.

[5] J.P. Fish and H.A. Carr, Sound Underwater Images: A guide to the generation and interpretation of sidescan sonar data, 2nd ed, Orleans, MA: Lower Cape Publishing, Orleans, 1991.

[6] D. Christie, Director of the NOAA West Coast and Polar Regions Undersea Research Center, personal communications, August 2010.

[7] “Mine warfare forces,” Jane’s Fighting Ships, S. Saunders, ed., Surrey, UK: Jane’s Information Group, 2004, pp. 177-18, 268-269, 706-707.

[8] V. Bertram, V., “Unmanned surface vehicles - A survey,” In Skibsteknisk Selskab, Copenhagen, Denmark, 2008. Available online at: http://www.skibstekniskselskab.dk/public/dokumenter/Skibsteknisk/Download%20materiale/2008/10%20marts%2008/USVsurvey_DTU.pdf

[9] J.E. Manley, "Unmanned surface vehicles, 15 years of development," Proceedings of MTS/IEEE OCEANS, Kobe, Japan, 2008, pp.1-4.

[10] M. Caccia, “Autonomous Surface Craft: prototypes and basic research issues,” Proceedings of the 14th Mediterranean Conference on Control and Automation, Ancona, Italy, 2006, pp. 1-6.

[11] Claudia Doria Rodriguez-Ortiz, “Automated bathymetry mapping using an autonomous surface craft,” M. S. Thesis, Dept. Ocean Engineering, Massachusetts Institute of Technology, MA, June 1996.

[12] Justin E. Manley, “High fidelity hydrographic surveys using an autonomous surface craft,” M. S. Thesis, Dept. Ocean Engineering, Massachusetts Institute of Technology, MA, June 1998.

[13] J. Manley, “Development of the autonomous surface craft ACES,” Proceedings of Oceans, vol 2, 1997, pp. 827-832.

[14] W. Naeem, T. Xu, R. Sutton, J. Chudley, “Design of an Unmanned Catamaran with Pollutant Tracking and Surveying Capabilities,” Proceedings of the UKACC Controls Conference, Mini Symposium on Marine Systems, Glasgow, UK, 2006, pp. 99-113.

[15] J. Majohr, T. Buch, and C. Korte, “Navigation and automatic control of the Measuring Dolphin (MESSIN),” Proceedings of the 5th IFAC Conference on Maneuvering and Control of Marine Craft, Aalborg, Denmark, 2000, pp. 405-410.

[16] Wen-Rong Yang, Cing-Ying Chen, Chao-Min Hsu, Chiung-Jung Tseng, and Wen-Chang Yang, “Multifunctional Inshore Survey Platform with Unmanned Surface Vehicles,” Proceedings of International Journal of Automation and Smart Technology, 2011, Vol 1, No 2.

[17] A. Martins, H. Ferreira, C. Almeida, H. Silva, J.M. Almeida, and E. Silva, "ROAZ and ROAZ II Autonomous Surface Vehicle Design and Implementation", Proceedings of the International Lifesaving Congress, La Coruna, Spain, 2007, pp. 1-7.

[18] M. Caccia, R. Bono, G. Bruzzone, G. Bruzzone, E. Spirandelli, G. Veruggio, A. Stortini, and G. Capodaglio, “Sampling sea surface with SESAMO,” IEEE Robotics and Automation Magazine, vol 12, no 3, 2005, pp. 95–105.

[19] J. Alves, P. Oliveira, R. Oliveira, A. Pascoal, M. Rufino, L. Sebastiao, and C. Silvestre, "Vehicle and Mission Control of the DELFIM Autonomous Surface Craft," Proceedings of the 14th Mediterranean Conference on Control and Automation, Ancona, Italy, 2006, pp. 1-6.

[20] W Naeem, T Xu, R Sutton, A Tiano, "The design of a navigation, guidance, and control system for an unmanned surface vehicle for environmental monitoring," Proceedings of the Institution of Mechanical Engineers, Part M: Journal of Engineering for the Maritime Environment, vol 222, no 2, 2008, pp. 67-79.

[21] J. Majohr and T. Buch, "Modeling, simulation and control of an autonomous surface marine vehicle for surveying applications: Measuring Dolphin MESSIN," Advances in unmanned marine vehicles, G.N. Roberts and R. Sutton, eds, Herts, UK: The Institution of Electrical Engineers, 2006, pp. 329–352.

[22] M. Bibuli, F. Bruzzone, M. Caccia, and L. Lapierre, "Path-Following Algorithms and Experiments for an Unmanned Surface Vehicle," Journal of Field Robotics, vol 26, no 8, 2009, pp. 669-688.

[23] A. Pascoal, C. Silvestre, and P. Oliveira, "Vehicle and mission control of single and multiple autonomous marine robots," Advances in unmanned marine vehicles, G.N. Roberts and R. Sutton, eds, Herts, UK: The Institution of Electrical Engineers, 2006, pp. 353-386.

[24] C. Almeida, T. Franco, H. Ferreira, A. Martins, R. Santos, J. Almeida, J. Carvalho, E. Silva, "Radar based collision detection developments on USV ROAZ II", Proceedings of Oceans 2009 Europe, Breman, Germany, 2009, pp. 1-6.

[25] P. Mahacek, "Dynamic Analysis of a SWATH Vessel," MBARI Internship Report, 2005, pp. 1-13. Available online at: http://www.mbari.org/education/internship/05interns/05papers/PMahacek.pdf, Accessed July 2011.

[26] J. Herring, C. Johnson, D. Moomaw, and J. Pool, "The SeaWASP: An Autonomous Multi-Payload Research Vessel," Adv. C. Kitts, Bachelor Project, Dept. Mech Engineering, Santa Clara University, CA. June 2010.

[27] R. Dinsmore, "Small SWATH Research Vessels," in UNOLS Small Research Vessel Compendium, J. Bash,ed., 2004. Available online at: http://www.unols.org/publications/manuals/SBCompendium/index.html, retrieved May 2011.

[28] Hart, "Measurements During SWATH Ship Sea Trials," IEEE Instrumentation and Measurement Magazine, vol 3, no 3, 2000, pp. 38-43.

[29] T. Nagai, "Critical Review of SWATH Vessels," Research Reports of Ikutoku Technical University, Part B Science and Technology B(11), 1987, pp. 1-21.

[30] A. Nelson, "Vessel." U.S. Patent 795,002, issues July 18, 1905.

[31] R. Gaul and A. McClure, "Development of the SWATH Ship Concept for Research Ship Design, Proceedings of Oceans, 1984, pp. 902-907.

[32] T. Lang, C. Bishop, and W. Sturgeon, "SWATH ship designs for oceanographic research," Proceedings of Oceans, 1988, pp. 1163-1168.

[33] R.L. Schaffer, J.A. Kupersmith, R. Wilson, and T.J. Valsi, "Explosive Ordnance Disposal Swath Ship Design," Marine Technology, vol 28, no 4, 1991, pp. 181-196.

[34] J. McCoy and W. Neely, "The SWATH Mine Hunter: An Enabling Technology That Works," Proceedings of the Fourth International Symposium on Technology and the Mind Problem, Naval Postgraduate School, Monterey, CA, 2000, pp. 11-13.

[35] H.H. Chun, M.S. Kim, and Y.R. Joo, "Seakeeping analysis of a 30-knot coastal passenger SWATH ship," Proceedings of the International Offshore and Polar Engineering Conference, vol 4, 1997, pp. 736-741.

[36] “R/V Kilo Moana cruise KM0206 to the Northwestern Hawaiian Islands Coral Reef Ecosystem Reserve,” Data Processing Excerpts from the cruise report, Oct-Nov 2002. Also available at: http://oceanexplorer.noaa.gov/technology/vessels/kilo/kilo.html

[37] C. Kitts, P. Mahacek, T. Adamek, K. Rasal, V. Howard, S. Li, A. Badaoui, W. Kirkwood, G. Wheat, S. Hulme, “Field operation of a robotic small waterplane area twin hull boat for shallow-water bathymetric characterization,” Journal of Field Robotics vol 29, issue 6, Nov-Dec 2012, pg 924-938.

[38] C. Kitts. "Surf, Turf, and Above the Earth: An Aggressive Robotics Development Program for Integrative Undergraduate Education." IEEE Robotics and Automation Magazine, v 10, n 3, 2003, pp. 30-36.

[39] E. Beck, W. Kirkwood, D. Caress, T. Berk, P. Mahacek, K. Brashem, J. Acain, V. Reddy, C. Kitts, J. Skutnik and G. Wheat. "SeaWASP: A Small Waterplane Area Twin Hull Autonomous Platform for Shallow Water Mapping." Marine Tech Soc Journal, v 43, n 1, 2009, pp. 6-12.

[40] Fossen, Thor I., Guidance and Control of Ocean Vehicles, Wiley, New York, 1994.

[41] D.W. Caress, H. Thomas, W.J. Kirkwood, R. McEwen, R. Henthorn, D.A. Clague, C.K. Paull, J. Paduan, and K. L. Maier, “High-Resolution Multibeam, Sidescan, and Subbomt Surveys Using the MBARI AUV D. Allan B.,” Proceedings of the Marine Habitat Mapping Technology for Alaska Workshop, Anchorage AK, 2007, pp. 47-69.

[42] J. G. Moore, R. A. Schweickert, J. E. Robinson, M. M. Lahren, and C. A. Kitts. “Tsunami-generated boulder ridges in Lake Tahoe, California-Nevada.” Geology, v 34, n 11, 2006, pp. 965-968.

[43] V. Howard, “Gradient following Tracking for Mobile Multi-robot Systems,” C. Kitts, Adv. M.S.Thesis, Dept. Mech Eng, Santa Clara University, Santa Clara, CA, 2010.

[44] T. Adamek, “Cluster Space Gradient Contour Tracking for Mobile Multi-robot Systems,” C. Kitts, Adv. M.S.Thesis, Dept. Mech Eng, Santa Clara University, Santa Clara, CA, 2010.

Appendix A: Simulink Model for Mow-the-Lawn with Feed-forward controller

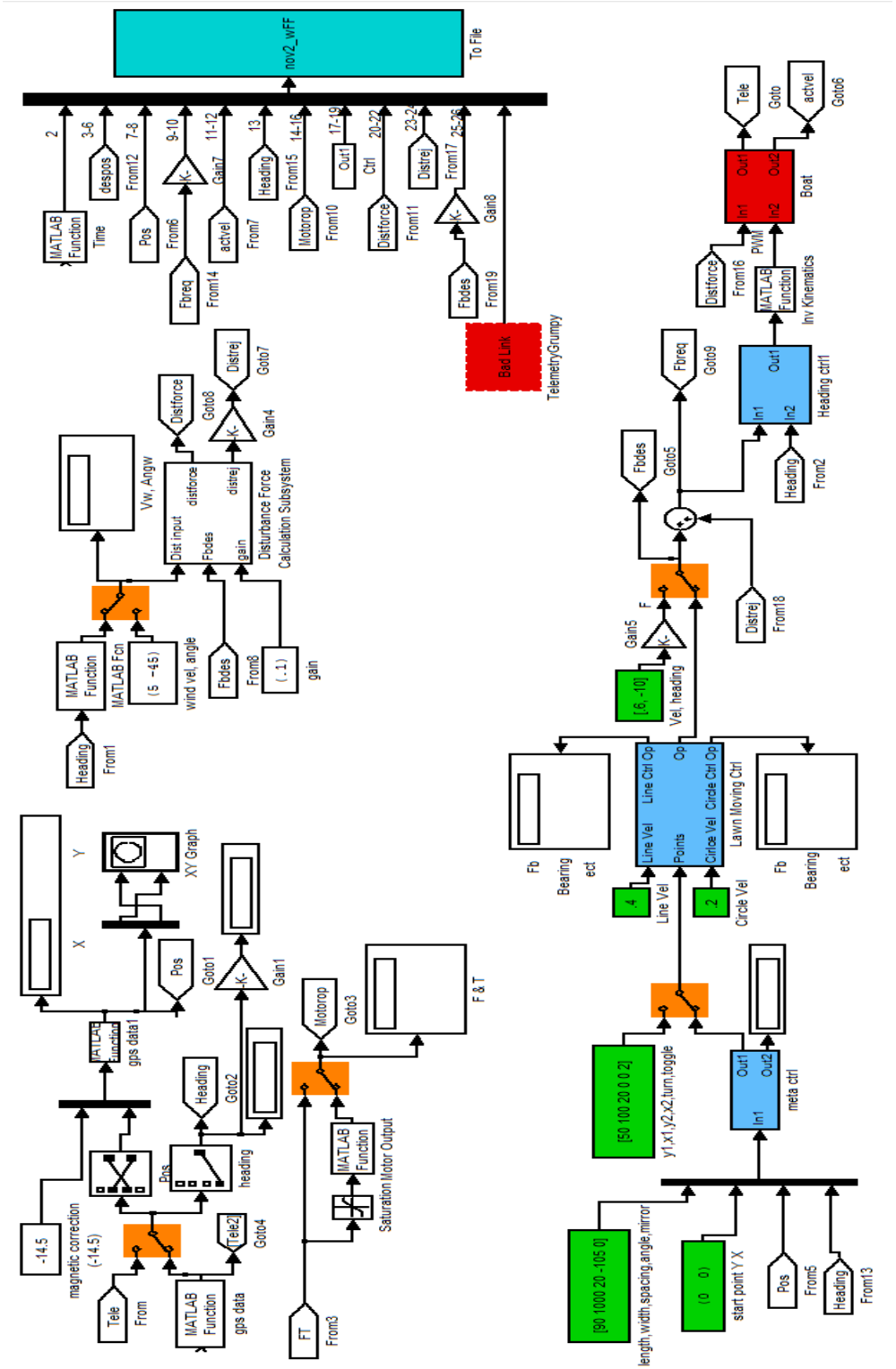

Appendix B: Subsystems of Model

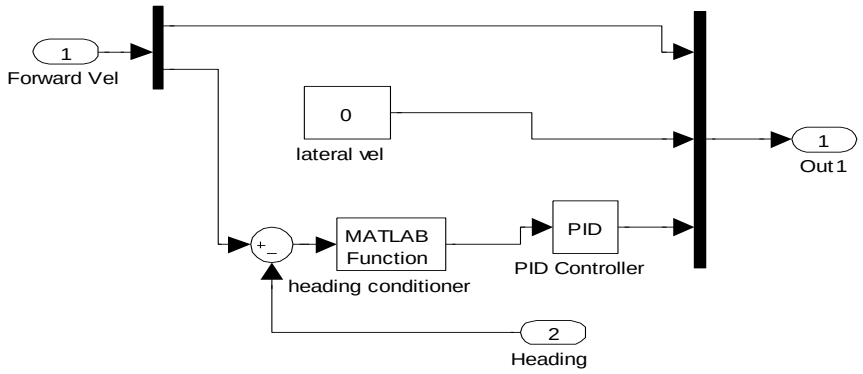

Heading Controller Subsystem

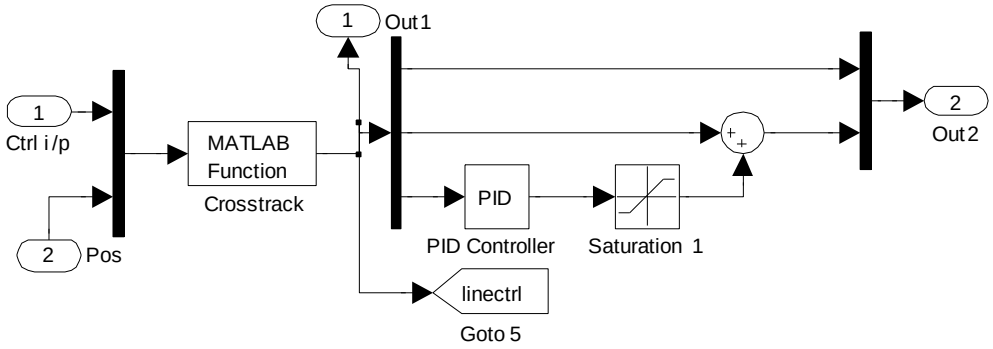

Line Controller Subsystem

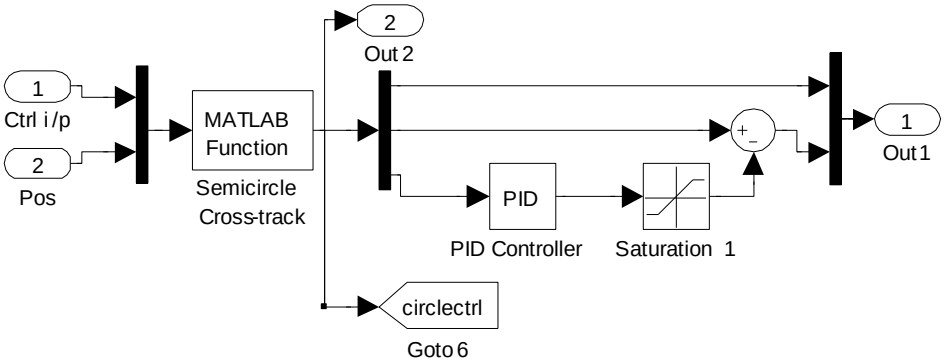

Circle Controller Subsystem

Appendix C: Simulink Model for Canard System

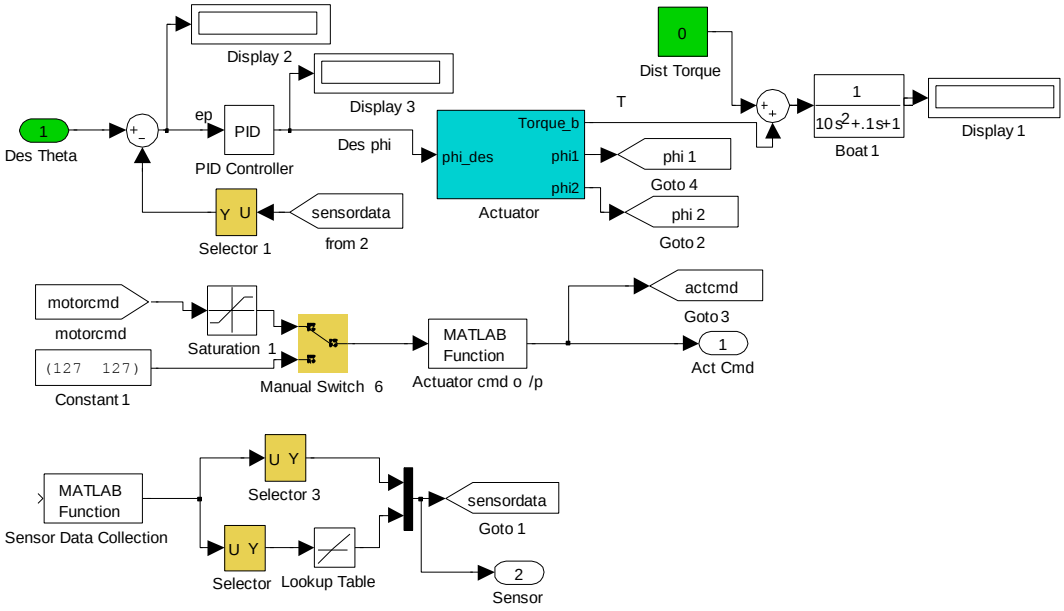

Canard Simulink Model

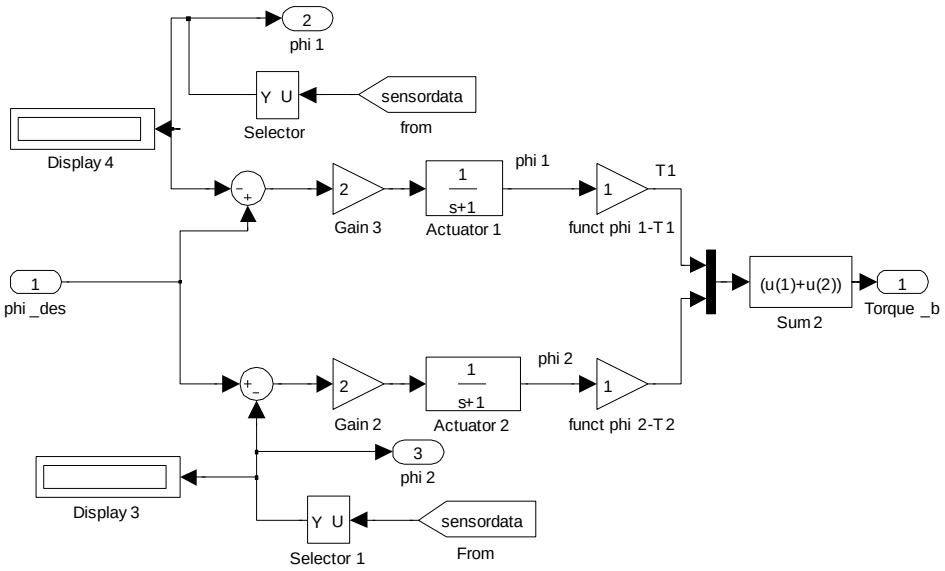

Actuator Subsystem